Impact of high-resolution Sea Surface Temperature representation on the forecast of small Mediterranean catchments hydrological response to heavy precipitation

Alfonso Senatore[1], Luca Furnari[1], Giuseppe Mendicino[1]

1 Department of Environmental and Chemical Engineering, Università della Calabria, P.te P. Bucci 42b, 87036 Rende (CS), Italy

Correspondence to: Alfonso Senatore (alfonso.senatore@unical.it)

Abstract. Operational meteo-hydrological forecasting chains are affected by many sources of uncertainty. In coastal areas characterized by complex topography, with several medium-to-small size catchments, quantitative precipitation forecast becomes even more challenging due to the interaction of intense air-sea exchanges with coastal orography. For such areas, quite common in the Mediterranean basin, improved representation of Sea Surface Temperature (SST) space-time patterns can be particularly important. The paper focuses on the relative impact of different resolutions of SST representation on regional operational forecasting chains (up to river discharge estimates) over coastal Mediterranean catchments, with respect to other two fundamental options while setting up the system, i.e., the choice of the forcing GCM and the possible use of a three-dimensional variational assimilation (3DVAR) scheme. Two different kinds of severe hydro-meteorological events affecting the Calabria Region (Southern Italy) on 2015 are analysed using the atmosphere-hydrology modelling system WRF-Hydro in its uncoupled version. Both the events are modelled using the 0.25° resolution Global Forecasting System (GFS) and the ECMWF's 16 km resolution Integrated Forecasting System (IFS) initial and lateral atmospheric boundary conditions, applying the WRF mesoscale model for the dynamical downscaling. For the IFS-driven forecasts, also the effects of the 3DVAR scheme are analysed. Finally, native initial and lower boundary SST data are replaced with data from the Medspiration Project by IFREMER/CERSAT, having a 24 hour time resolution and 2.2 km spatial resolution. Precipitation estimates are compared with both ground-based and radar data, as well as discharge estimates with stream gauging stations data. Overall, the experiments highlight that the added value of high-resolution SST representation can be hidden by other more relevant sources of uncertainty, especially the choice of the General Circulation Model providing boundary conditions. Nevertheless, high-resolution SST fields show in most cases a not negligible impact on the simulation of the atmospheric boundary layer processes, modifying flow dynamics and/or the amount of precipitated water, therefore emphasizing that uncertainty in SST representation should be duly taken into account in coastal areas operational forecasting.

1 INTRODUCTION

Operational river flood forecasting is a highly challenging activity for several reasons that go beyond strictly scientific aspects. Hydrometeorological forecasting requires extremely complex systems, where issues like communication of warning,

accessibility of the results and administrative and/or institutional factors can be as important as monitoring and modelling activities (Pagano et al., 2014; Silvestro et al., 2017). Nevertheless, the cornerstone of such systems, and undoubtedly the most demanding part from a scientific point of view, still is the meteorological-hydrological modelling chain, supported by in-situ or remotely sensed measurements.

Increasingly refined modelling chains have been developed in the recent years (e.g., UK Environmental Prediction Research; Lewis et al., 2019a; Canadian Great Lakes; Gronewold et al., 2011; U.S. Navy's Coupled Ocean/Atmosphere Mesoscale Prediction System COAMPS®; Hodur, 1997). Despite their complexity, these systems all have to deal with some inherent limitations of the meteorological and hydrological models. The main sources of errors in weather forecast are connected to both inaccuracy in defining the initial state, due to the lack of available measures or observation/assimilation errors, and approximations of the models, whose structure is not capable to represent properly the phenomena of interest (Allen et al., 2002; Buizza, 2018). These problems are exacerbated by the chaotic nature of the atmosphere. Even though hydrological models are much simpler than meteorological models in their structure (Liu et al., 2012; Pagano et al., 2014), they also have to struggle with different sources of uncertainty that, according to Renard et al. (2010), can be grouped in four categories: 1) input uncertainty; 2) output uncertainty (e.g., runoff estimates are not straightforward); 3) structural model uncertainty and; 4) parametric uncertainty. Furthermore, since very seldom catchments are perfect natural systems, some effects of human disturbances virtually cannot be modelled.

The main link between atmospheric and hydrological compartments in a forecasting chain is precipitation forecast, which is an output variable for weather models and constitutes the main input for hydrological models. Quantitative Precipitation Forecast (QPF) is a major challenge for operational meteorology, because the reliability of precipitation forecasts crucially affects streamflow forecasts skill (for a review see Cuo et al., 2011; for recent applications, e.g., Davolio et al., 2015; Tao et al., 2016; Davolio et al., 2017; Li et al., 2017). Among the various strategies adopted for addressing this issue, several studies focusing on coastal areas assessed in the recent years the importance of Sea Surface Temperature (SST) initial and boundary conditions as relevant drivers of QPF, capable to influence, consequently, the streamflow forecast. This impact can be particularly strong in topographically complex coastal areas, characterized by several small catchments, such as in the Mediterranean Basin, for which several cooperative research efforts have been activated (e.g., the MEDiterranean Experiment, MEDEX; Jansa et al., 2014; the HYdrological cycle in the Mediterranean Experiment, HyMeX; Drobinski et al., 2018).

Several studies focused recently on the effects of sea surface-atmosphere interactions over heavy precipitation at mid-latitudes, particularly in the Mediterranean area (e.g., Manzato et al., 2015; Romaniello et al., 2015; Rainaud et al., 2016). Some of them showed that large variations of the average values of SST boundary conditions significantly affect location and intensity of high impact events (Lebeaupin et al., 2006; Miglietta et al., 2011; Senatore et al., 2014; Meredith et al., 2015; Pastor et al., 2015; Miglietta et al., 2017; Pytharoulis, 2018). Furthermore, using coupled atmosphere-ocean simulations, Berthou et al. (2014, 2015) highlighted the major effects of long-term SST changes in the representation of Mediterranean intense rain events, even though features at smaller time scales can also contribute significantly. Lebeaupin et al. (2006) found that higher resolution SST fields have poor effects on convection in the case study they analysed (southern France). Ivatek-Šahdan et al.

(2018), examining several events in the Eastern Adriatic, also found that more realistic SST fields did not substantially improve precipitation estimate; furthermore, they showed that the impact of high-resolution SST varied in different cases. Conversely, Katsafados et al. (2011) found noticeable deviations among the forecast skills of simulations with SST boundary conditions at different resolutions in a test-case in the Eastern Mediterranean, while Cassola et al. (2016) verified in a study in north-western Italy that high-resolution SST fields can positively impact QPF in the forecasting range 36-48 h. Finally, Berthou et al. (2016) in southern France and Stocchi and Davolio (2017) in the Adriatic Sea highlighted that SST-atmosphere interactions affect precipitation patterns and intensity mainly through complex (and varying event-by-event) modifications of the stability of the upstream atmospheric boundary layer.

The main objective of this paper is to contribute to the current discussion on the impact of SST representation by extending the analysis over the whole meteo-hydrological forecasting chain, i.e. going beyond precipitation forecasts and evaluating sensitivity on streamflow forecasts. Furthermore, SST sensitivity is assessed in the context of the overall uncertainty linked to initial and boundary conditions in regional modelling, using different forcing GCMs, with and without data assimilation. To this aim, different accuracy levels of SST representation are used in an operational meteorological-hydrological forecasting chain over a coastal Mediterranean area including, in addition to the native SST fields of the General Circulation Models (GCMs), also higher resolution fields (namely, the Medspiration level 4 Ultra-High Resolution foundation SST -SSTfnd- from the Medspiration Project by the Centre European Remote Sensing d'Archivage et de Traitement -CERSAT- Institut Français de Recherche pour L'Exploitation de la Mer –IFREMER; Merchant et al., 2008; Robinson et al., 2012). Furthermore, two GCM forecasts are used (namely, the Global Forecasting System -GFS- provided by the US National Weather Service -NWS- and the Integrated Forecasting System -IFS- developed at the European Centre for Medium-Range Weather Forecasts - ECMWF) and a three-dimensional variational assimilation (3DVAR) scheme.

The study area, corresponding to the Calabrian peninsula (southern Italy), due to its particular position in the middle of the Mediterranean Sea and its complex and steep orography experiences quite regularly severe precipitation events and is particularly prone to significant ground effects (Federico et al., 2003a, 2003b; Federico et al., 2008; Chiaravalloti and Gabriele, 2009; Llasat et al., 2013; Gascòn et al., 2016; Avolio and Federico, 2018; up to a very recent flash flood that on 20 August 2018 caused 10 casualties; Avolio et al., 2019). According to Avolio and Federico (2018), severe precipitation events over Calabria can be classified in short-lived events, lasting less than 24 hours, and long-lived events. Following this classification, in this paper, two case studies occurred in 2015 are considered, the former characterized by convective, very localized precipitation (11-12 August; CFM, 2015a) and the latter by more persistent and widespread stratiform precipitation (30 October – 2 November; CFM, 2015b).

The meteorological-hydrological forecasting chain is based on the WRF-Hydro modelling system (Gochis et al., 2015). This open-source community model, originally developed as the hydrological extension of the Weather Research and Forecast (WRF; Skamarock et al., 2008) model, provides a coupling architecture allowing to connect vertical water fluxes between the earth surface and the atmosphere, simulated at coarse resolution by the atmospheric model, to lateral surface and sub-surface fluxes simulated at high-resolution by the hydrological model, both in one-way (i.e., with no feedback from the routing models

to the atmosphere) and two-way (with feedback) manner. WRF-Hydro system dramatically evolved in last years (Salas et al., 2018; Lin et al., 2018: Lahmers et al., 2019), being operationally adopted into the NOAA National Water Model (NWM, Cohen et al., 2018) across the continental U.S, besides being used for research applications (e.g., Yucel et al., 2015; Senatore et al., 2015; Arnault et al., 2016; Verri et al., 2017).

The paper is organized as follows. Section 2 describes the study area, the two events analysed, the numerical model and its setup with details on space and time resolutions of the boundary conditions. In Section 3 the results of the meteorological and hydrological outputs are analysed separately for the two events. Finally, Section 4 discusses and summarizes the main findings and outlines future research lines.

2. MATERIALS AND METHODS

2.1 Study area and events description

Calabria is a peninsula characterized by a complex orography. Its geographical and morphological features produce a very irregular precipitation distribution (average annual precipitation varies between 600 and 1500 mm; Federico et al., 2010) and foster the occurrence of extreme weather events, which often caused deaths (Petrucci et al., 2018). Among the relatively numerous recent events, this study focuses on two case studies occurred in 2015 and characterized by distinctive features.

The first high impact event (case study 1) was very localized in space and time and hit the north-eastern part of the region on the morning of 12 August 2015. The analysis at the synoptic scale (Figs. 1a-b) shows that in the early hours of 12 August 2015 a main low-pressure system coming from the Atlantic moved over the French and Spanish coasts, while over the central Mediterranean a cut-off low occurred, giving rise to a new low-pressure vortex with reduced dimensions that caused intense local rainfall. The observed precipitation patterns (Fig. 1c) involved only small areas in the mainland, specifically the territory of the Corigliano and Rossano municipalities. The data provided by the Italian National Radar Network (integrated into the same map of Fig. 1c), though underestimating ground observations, show that most of the precipitation occurred over the Ionian Sea. The Corigliano rain gauge measured high rainfall values (Fig. 1d). During the 48 hours from 00:00 UTC 11 August 2015 up to 00:00 UTC 13 August 2015, 255.2 mm of rain were recorded, with a maximum of 246.4 mm in 24 hours (from 18:00 UTC 11 August to 18:00 UTC 12 August), 223.2 mm in 12 hours (from 01:45 UTC 12 August to 13:45 UTC 12 August), 167.4 mm in 6 hours, 107.2 mm in 3 hours and 51.4 mm in 1 hour. The hydrological impact concerned some small/very small coastal catchments, the most important of which is the Citrea Creek (11.4 km^2, catchment boundaries highlighted in Fig. 1e), which overflowed causing several tens of millions of euros of damage.

The second event (case study 2) involved a much larger area and developed over 4 days, from 30 October to 2 November 2015. The synoptic analysis (Fig. 2e) shows another cut-off low, remaining stationary over Sicily for much of the period and attracting humid and warm air from the Ionian Sea to the southeast (a detailed synoptic description of the event is provided by Avolio and Federico, 2018). The orographic effect in this event turned out to be decisive, the Calabrian mountain ranges acting

as a real barrier, therefore a large part of the rainfall occurred in the Ionian (eastern) side of the region. While on 30 October 2015 only the northern part of the region was affected (Fig. 2a; about 200 mm in 24 hours in the Oriolo station), the highest precipitation during the entire event was recorded in the southern coast (Figs. 2b-d), with a maximum of about 740 mm (Chiaravalle Centrale station) and a daily maximum of about 370 mm (Sant'Agata del Bianco). In Figs. 2a-d, rain gauges observations overlap the precipitation fields detected by the weather radars, extending also over the sea. The hydrological impact of the event concerned the whole eastern side of the region. Two catchments are selected for this study, namely the Ancinale River closed at the Razzona gauging station (116 km^2, Fig. 2f) and the Bonamico Creek closed at the Casignana gauging station (138 km^2, Fig. 2g). Such catchments are chosen because they are two of the biggest with available observations of water levels (unfortunately no discharge data are available) and are located in the north and the south, respectively, of the rainiest area. Specifically, Chiaravalle Centrale station is located at the Ancinale River outlet.

2.2 Numerical model description and setup

2.2.1 WRF

The Advanced Research WRF (ARW) Model, version 3.7.1, is used in two one-way nested domains (Fig. 3). The external domain D01 covers a large area of the Mediterranean (33.04°-49.85°N, 3.59°-28.59°E) with a 10 km (187 × 205 grid points) horizontal resolution, while the innermost domain D02 is centred over the Calabrian peninsula (37.10°-40.87°N, 13.88°-18.71°E), with a 2 km (200 × 200 grid points) horizontal resolution. The model runs on 44 vertical atmospheric layers, up to a 50-hPa pressure top (about 20000 m), and on 4 soil layers, down to 2 m below the surface. The time step of the model simulation is 60 s in D01 and 12 s in D02.

Physical parameterization of the model is the same used by Senatore et al. (2014) and is reported in Table 1. Boundary and initial conditions are provided by two operational forecast GCMs, namely the GFS in forecast mode with a spatial resolution of 0.25° (about 27 km) and the IFS-ECMWF High RESolution (HRES) in forecast mode with a spatial resolution of about 16 km. In both cases, boundary conditions are provided every 6 hours. As a further step, both initial and lower boundary SST data are replaced with the Medspiration L4 Ultra-High Resolution SSTfnd (obtained as daily mean with a resolution of 0.022°). The high-resolution Medspiration SST fields are ingested through GIS-based techniques into the WRF initial and lower boundary conditions files of both domains following Senatore et al. (2014).

Furthermore, two relevant options allowed by the WRF modelling system are always activated for all SST boundary conditions: the *sst_update* option, allowing dynamical lower boundary (i.e., SST) conditions, and the *sst_skin* option, based on Zeng and Beljaars (2005), which permits the simulation of SST dynamics. It is noteworthy that the higher resolution of the SST fields does not imply a greater accuracy, which can be objectively assessed through a comparison with in-situ observations. For this purpose, a preliminary search is performed in the Copernicus Marine Environment Monitoring Service (CMEMS), in particular in the CORA database (Cabanes et al., 2013) in the latest version released (5.2, April 2019). Useful

data (i.e., continuous measurements with a sub-daily time step at the sea-surface interface) are found only rather at the border of the external domain D01 for both the case studies (Fig. S1a in the Supplement).

Finally, both as an additional comparison and with the aim of highlighting its relative impact with respect to the effects of different boundary conditions provided by different GCMs and/or more detailed SST fields, also a data assimilation technique is used for both the test cases. Specifically, a 3DVAR assimilation scheme (Barker et al., 2004; Huang et al., 2009; Barker et al., 2012) is adopted, introducing conventional meteorological observations into the initial conditions and adjusting boundary conditions to improve simulations performance.

A summary of all simulations carried out is reported in Table 2.

2.2.2 WRF-Hydro

In this work, WRF-Hydro version 3.0 is used in one-way mode. Therefore, the atmospheric model outputs are used as input of the hydrological model using an hourly time step. According to the WRF parameterization, the Land Surface Model (LSM) is Unified Noah and is used at the same resolution of the domain D02, while for the lateral routing of surface and subsurface water an increased horizontal resolution of 200 m is used (2000 × 2000 grid points), thus having an aggregation factor of 1 / 10 from the atmospheric to the hydrological model.

No observed discharge or flow depth data is available for case study 1, hence model calibration is not performed. In case study 2, model calibration is performed manually with respect to the available water level data for the two selected catchments (Ancinale and Bonamico), with the aim of reproducing the timing of the hydrological responses to heavy precipitation and, mainly, to correctly simulate the peak flow time, which is a paramount variable for civil protection activities.

The humidity and temperature conditions in the 4 soil layers at the beginning of the analysed event (30 October 2015 00:00 UTC) are achieved through off-line simulations with a spin-up time of one month. The meteorological forcing for this period is basically given by the spatial interpolation of ground-based observations (provided by the monitoring network managed by the Centro Funzionale Multirischi-ARPACAL, Calabria Region). The interpolation techniques adopted are the same described in Senatore et al. (2015) except that precipitation fields are interpolated through Inverse Distance Weighting (IDW) instead of exponential kriging. Furthermore, only during the event (i.e., from 30 October to 2 November 2015) precipitation fields (Figs. 4a-b) are achieved merging hourly ground-based rainfall observations to hourly radar data estimates provided by the Italian weather radar network managed by the National Department of Civil Protection. The merging procedure follows Sinclair and Pergram (2005) with the difference that, instead of a double kriging interpolation, a simpler double IDW interpolation method is used. The merging technique guarantees an increase of the total “observed” rainfall volume, with respect to a simple IDW interpolation, of +4.6% over the Ancinale River and +10.6% over the Bonamico Creek.

The parameters involved in the calibration procedure are broadly the same used in previous studies with WRF-Hydro (e.g., Yucel et al., 2015; Senatore et al., 2015). Specifically, the LSM parameters calibrated are the infiltration factor (REFKDT), the coefficient governing deep drainage (SLOPE) and the thicknesses of the 4 soil layers. In addition, two spatially distributed

parameters of the hydrological model, namely the overland flow roughness scaling factor (OVROUGHRTFAC) and the initial retention height scaling factor (RETDEPRTFAC), are calibrated together with the Manning roughness coefficients (one value for each stream order).

The calibrated parameters are shown in Table 3 while resulting hydrographs are shown in Figs. 4c-d together with uncalibrated hydrographs. The more impulsive behaviour of the Bonamico Creek, typical of Calabrian "fiumare", is simulated through lower values of the infiltration factor and lower soil layers thickness. Nevertheless, in order to allow timely peak flows simulation, a small delay of the initial response is necessary through an increase in the RETDEPRTFAC value, which is compatible with noteworthy initial ponding in the wide alluvial bed and infiltration in the gravelly soil. On the other hand, abundance of organic matter in the soils of the dense forests within the Ancinale River catchment, which especially in autumn can store considerable quantities of water, most probably contributes substantially to the smoother response of the Ancinale River. Figs. 4c-d highlight that the calibration procedure mainly influences the results concerning the Ancinale River, especially in terms of total volumes.

As for the hydrographs, adopting typical stage-discharge power relationships (i.e., $q = a \cdot h^b$, where q is the discharge, h the water level and a and b two calibration coefficients) the coefficients of determination (R^2) between simulated discharge values and observed water levels are equal to 0.942 and 0.831, respectively for the Ancinale River and the Bonamico Creek. Concerning the reliability of the simulated discharge amount, since reference observations are missing, an indirect validation of the peak flows achieved is performed using the Hydrologic Engineering Center's (CEIWR-HEC) River Analysis System (HEC-RAS) (Hydrologic Engineering Center, 2016). Cross-sections, for both the outlets of the catchments and for 4 upstream and downstream points approximately spaced 50 m, are determined merging data from a ultra-high-resolution (5 m) Digital Terrain Model provided by the Calabria Region Cartographic Centre with the heights given in very recent official maps (Technical Cartography of Calabria Region) at a scale of 1:5000. Such cross-sections are further validated by on-field sample measurements. One-dimensional steady flow simulations reaching observed peak heights provide peak discharges broadly comparable to the results achieved with the model.

For the sake of brevity, hereafter the WRF-Hydro hydrographs calibrated using observed precipitation fields shown in Fig. 4 will be referred to as 'observed hydrographs' or simply 'observations'.

3. RESULTS AND DISCUSSION

3.1 Case Study 1

The analysis with the CORA database (Figs. S1b-d) shows that Medspiration-derived lower boundary conditions, though originating from a high-resolution dataset, do not provide a clear improvement of skin SST representation compared to the original GCM fields. It is to be noticed, however, that the SST boundary conditions in D01 are aggregated at a 10 km resolution. Panels in Fig. S2 focus on the Domain D02 and show, for all simulations carried out in this case study, the skin SST fields from 11 August 18:00 UTC to 12 August 18:00 UTC with a time step of six hours. The main features highlighted by the skin

SST maps are the strong underestimation of native IFS fields close to the coastline (this is due to a known interpolation problem along coastlines that lowers temperatures to unrealistic values; L. Magnusson, personal communication) and the overestimation, especially off the Tyrrhenian Sea (up to more than 2 K), of the native GFS fields. The other skin SST fields mostly differ each other less than ±0.5 K. It is noteworthy that skin SST fields in the simulations using Medspiration product are not identical due to the fact that, with the method of Zeng and Beljaars (2005), skin SST values are influenced by the surface winds and net radiation fluxes modelled by the different simulations.

A comparison of the time evolution of the average skin SST values in the whole domain D02 would be biased by the not negligible IFS underestimation near the coastline. Instead, an analysis performed on selected significant points could provide more interesting insights. For this reason, focusing on the Ionian Sea, in Fig. 5 the points 1, closer to Corigliano-Rossano, and 2, off the Calabrian southern coast (the exact location of both points is given in Fig. 3b), are examined. Concerning daily values, a clear but slight (<0.5 K) overestimation of GFS-O is shown for both days in point 1 and on the second day in point 2. Some hourly differences are more evident: e.g., in point 1 GFS-O values are up to 1.5 K higher than other models on 12 August at around 12:00, while in point 2 peak values of IFS-O and IFS-M on 11 August at around 12:00 are about 1 K higher than other models. Nevertheless, the differences among models during the night between 11 and 12 August (i.e., right before and during the rain event) are generally low. The only noteworthy difference is given, in point 2, by the small underestimation of Medspiration simulations (i.e., GFS-M, IFS-M and IFS-DA-M) of about 0.3-0.4 K, given by a sudden reduction of their skin SST values, most probably due to the change of the Medspiration SST field (from 11 August to 12 August). This behaviour, clearly not realistic, highlights a weakness occurring while ingesting directly such external data in the WRF simulation.

The accumulated precipitation modelled by all simulations for the 24-hour period from 11 August 18:00 UTC to 12 August 18:00 UTC is shown in Fig. 6. Overall, all models miss the location of the event, moving it further south, off the Ionian coasts. GFS-based simulations forecast more rainfall than IFS-based (average values in the domain of 10.1 mm and 8.9 mm with the native SST fields, 10.4 mm and 9.5 mm with the Medspiration SST fields, respectively for GFS and IFS), but more centred to the south. IFS-based simulations forecast rainfall clusters with more elongated shapes in the south-north direction, allowing more precipitation to reach the central-northern Ionian coasts (namely, the Corigliano-Rossano area). Even though simulations based on the 3DVAR scheme still miss the correct location of the event, they both provide more rainfall in the domain (average values of 11.2 mm with the native SST fields and 11.0 mm with the Medspiration SST fields) and show also a well-defined rainfall cluster close to the central Ionian coast. Both IFS and 3DVAR simulations overestimate land precipitation in that area. According to the generally small differences identified in the SST fields, Fig. 6 clearly shows that ingesting high-resolution SST information provides, in terms of spatial distribution of accumulated precipitation, much less relevant (and partially chaotic) effects than changing initial and boundary conditions or using data assimilation schemes, and a minor or possibly opposite impact on the accuracy of the simulations. Given the peculiar features of the analysed event, it makes sense to focus on the area surrounding the Corigliano gauge station. For each simulation, the graph in Fig. 7a merges intensity, location and time correlation information of the closest rainfall peaks (with a threshold of at least 40 mm) to that station, while Fig. 7b

explicitly shows the time evolution of accumulated rainfall for each of the locations identified (the points are highlighted with small stars in the panels of Fig. 6). Given that all simulations strongly underestimate the observed rainfall value of 246.4 mm (the highest simulated value of about 100 mm is given by IFS-DA-M), there is no configuration clearly over-performing the others. Both GFS peaks are located to the south (about 20 km) and delay the rain event from 8 (GFS-M) to 11 (GFS-O) hours. IFS-O and IFS-DA-O peaks are lower than IFS-M and IFS-DA-M, but they are generally closer to the Corigliano station (about 13 km and 22 km, respectively). Furthermore, Fig. 7b shows that ingesting Medspiration fields moves up the rainfall events for both IFS-O and IFS-DA-O. This suggests that removing the unrealistic low SST values along the coastline near the Corigliano station (i.e., considering IFS-M and IFS-DA-M in place of IFS-O and IFS-DA-O, respectively) produces the double effect of increasing rainfall amounts and accelerating flow dynamics. Such effect is more easily recognizable looking at the 3DVAR simulations, which provide more water vapour and precipitation. Moving from IFS-O to IFS-DA-O to IFS-DA-M, 850 hPa wind speed on 12 August at 00:00 UTC generally increases in domain D02 and specifically off the northern Ionian coasts of Calabria (Fig. S3). As a result, Fig. 8 shows that moving from IFS-O to IFS-DA-O to IFS-DA-M, the integrated water vapour (IWV) cluster off the Ionian Sea simulated three hours later (03:00 UTC) is both bigger and closer to the coast. Differences between IFS-O and IFS-DA-O are due to the assimilation in the domain D01 of 14 vertical profiles of pressure, wind speed and direction, absolute and dew point temperature and relative humidity, together with 14 point measurements provided by aircrafts at a fixed pressure level (corresponding to about 12 km). Instead, differences between IFS-DA-O and IFS-DA-M are mainly due to different skin SST values. Specifically, higher SST values given by ingesting Medspiration fields on the one hand enhance water vapour concentration in the atmosphere (the average upward moisture flux from sea surface in domain D01 increases of about 5%), on the other hand affect the stability of the atmospheric boundary layer, providing more energy to the system and accelerating the flow dynamics (such as found, e.g., by Stocchi and Davolio, 2017). The early arrival of the moist air mass towards the area of Corigliano-Rossano using Medspiration SST fields is highlighted by the time series of hourly averaged water vapour flux through section AA' (Fig. 9, with the Section shown in Fig. 3b). Local flow peaks are moved up from 2 to 4 hours in advance with IFS-DA-M compared to IFS-DA-O, and similar behaviour, even though less evident, is observed with IFS-M compared to IFS-O.

Concerning the assessment of the hydrological impact of the forecasted event, notwithstanding the detailed analysis performed, case study 1 does not provide relevant results (Table 4). The centre of the Citrea catchment is located 8 km approximately south-east of the Corigliano gauge station, has a maximum length of about 7 km in the south-north direction and a maximum width of only 2.5 km. The level of accuracy achieved by all simulations performed is not yet enough to correctly forecast the hydrological impact for such small catchments in areas with very complex topography like that analyzed. The maximum rainfall accumulated value over the catchment is forecasted by IFS-O, with 16 mm in 3 hours. However, the accuracy of the models is already high enough to make them very useful (it is worthwhile to recall that the starting time of the simulation is more than 24 hours before the event). In fact, if model forecasts are used for inferring information about wider 'warning areas' than single small catchments (such as the Italian Civil Protection system actually does), they provide essential inputs for civil protection activities.

3.2 Case Study 2

Case study 2 embraces a longer period than case study 1. In this Section, forecasting skills are assessed considering both the whole 4-day length of the event (i.e., from 30 October 2015) and a 3-day forecast starting on 31 October 2015, in order to reduce the uncertainties attributable to the longer lead time forecast.

Such as in the previous case study, the first analysis is devoted to skin SST fields. The comparison with the SST measurements available from the CORA database shows a much better behaviour of the Medspiration SST fields in the analysed region of the external domain (Figs. S1e-g). Focusing on the innermost domain, Fig. S4 highlights (besides the already mentioned IFS-related problem along coastlines) that, in this case, Medspiration fields for the whole period overestimate both GFS and IFS native SST fields. Specifically, average differences with respect to GFS SST vary from about 0.6 to 0.8 K, while differences with respect to IFS SST fields are higher than 0.8 K (the average difference increases to about 1.5 K if also the values along coastlines are considered). It is noteworthy that also GFS underestimates skin SST particularly near coastlines, while, such as in the previous test case, there is an overestimation off the Tyrrhenian Sea. Focusing on points 1 and 2 (Fig. 10) it is shown that: 1) both points replicate the general behaviour, with Medspiration fields values higher than GFS, in their turn higher than IFS; 2) differences are more marked in point 1 (average values of +1.0 and +0.6 K, respectively for IFS and GFS) than in point 2 (+0.9 and +0.3 K); 3) such as in the case study 1, also here, in the graph related to point 1, a sudden reduction of about 0.5 K can be observed for Medspiration, moving from 1 November to 2 November. Nevertheless, a similar abrupt change, even though less marked (about 0.2 K), is observed also for GFS on 31 October 06:00 UTC. Summarizing, this case study shows an evident skin SST increase from IFS to GFS to Medspiration.

Fig. 11 shows the accumulated rainfall fields in the 4-day simulation period by the 6 WRF configurations compared with a rainfall map of Calabria achieved merging ground measurements to radar observations (the merging procedure followed Sinclair and Pergram, 2005; distinct rain gauge and radar data are available in Figs. 2a-d). It clearly highlights, in agreement with the previous case study, that the main impact on rainfall output is given by the choice of the GCM providing boundary conditions. Average accumulated precipitation in domain D02 is equal to 80 mm with GFS-O, 71 mm with IFS-O and 68 mm with IFS-DA-O. Interestingly, the introduction of the 3DVAR scheme this time leads to reduced precipitation (in the domain D01 22 vertical profiles and 16 points measurements are assimilated). Higher skin SST values with Medspiration result in increased average precipitation in the domain D02 for all three cases, from +8% (IFS-DA) to +11% (GFS). Concerning the precipitation patterns, for the aims of this study, it is interesting to focus on the biggest cluster in the south-east corner of the domain (i.e., the direction from which the humid air mass comes). Moving from GFS to IFS to IFS-DA, quite independently from SST fields change, a shift of this cluster can be observed from north-east to south-west.

The main change produced by the 3-day forecast compared to the 4-day forecast is the higher correspondence of the GFS-based simulations to the IFS-based (Fig. S5). The GFS-based rainfall footprints located in the south-east of the domain D02 meet the Calabrian Ionian coast more southern with respect to the 4-day simulation, in agreement with the IFS-based

simulations. Overall, the simulated rainfall fields are rather similar to each other and seem to reproduce reasonably well the observations in the southern part of the region (i.e., the area most affected by the event), while the overforecast found in the 4-day simulation in the central zone is confirmed. 3DVAR forecasts starting on 31 October assimilate 15 vertical profiles and 12 point measurements. Though the IFS-based simulations forecast higher rainfall peaks off the southern Ionian coast (up to 1000 mm), the average accumulated precipitation in D02 is almost identical for all simulations (51 mm with GFS-O, 52 mm with IFS-O and 53 mm with IFS-DA-O). Precipitation increase caused by the higher skin SST Medspiration fields varies from +9% (IFS-DA) to +12% (GFS), in agreement with the upward moisture flux increase in D01 (+7% with GFS, +8% with IFS and IFS-DA).

With the aim of objectively assessing the performance of each WRF configuration, a detailed analysis using categorical scores is carried out considering ground-based observations in the Civil Protection warning areas more affected by the event (grey areas in the reproduction of the Calabria region in Fig. 12). Specifically, 30, 19 and 22 rain gauges are considered, respectively for zones Cala4, Cala7 and Cala8. Among the numerous scores available in the literature (for a review see, e.g., Wilks, 2006), for each zone Fig. 12 shows the results concerning the Frequency Bias Index (FBI):

$$FBI = \frac{hits + false\ alarms}{hits + misses} \quad (1)$$

and the Equitable Threat Score (ETS):

$$ETS = \frac{hits - hits_r}{hits + misses + false\ alarms + hits_r} \quad (2)$$

where

$$hits_r = \frac{(hits + misses)(hits + fase\ alarms)}{hits + misses + false\ alarms + correct\ negatives} \quad (3)$$

In the previous equations, the terms *hits*, *misses*, *false alarms* and *correct negatives* refer to a typical 2 × 2 contingency table. The FBI indicates if the forecast system has a tendency to underestimate (FBI<1) or overestimate (FBI>1) events frequency, while ETS measures the fraction of the correctly predicted events, adjusted for hits associated with random forecasts, and ranges from -1/3 to 1 (perfect score). Both scores are used for consecutive 6-hour time intervals for the analysed rainy period, using precipitation thresholds with a step of 0.2 mm from 0.2 to 1 mm, a step of 1 mm up to 10 mm, a step of 2 mm up to 20 mm and a step of 5 mm for higher rates.

Focusing on the 4-day simulations, ETS graphs show the generally better performance of IFS-DA-M, especially for higher thresholds. Other models have discording levels of accuracy: e.g., IFS-DA-O is the best in Cala4, but the worst in Cala7. Nevertheless, ingesting high-resolution SST generally provides better scores in all cases. Complementary information provided by FBI highlights significant underforecast of GFS-based simulations in both Cala4 and Cala8 and overforecast in Cala7. Other simulations behave better, but also FBI points out that the 3DVAR scheme alone does not necessarily improve IFS-based forecasts (e.g., in Cala7 IFS-O is more accurate than IFS-DA-O), unless also a high-resolution SST representation is considered (IFS-DA-M always shows FBI values around 1). The ETS values of the 3-day simulations are generally higher, but, in this case, the GFS-based simulations are the worst, and introducing the Medspiration fields further reduces their performance. On the other hand, a more detailed SST resolution increases the ETS values of the IFS-based simulations in zones Cala4 and Cala8

(but not in zone Cala7). Concerning bias, FBI graphs show substantial underforecasts in zones Cala4 and Cala8 and overforecast in zone Cala7. However, in this case, the GFS-based simulations provide better results, especially in zone Cala7 and for high thresholds. Results achieved with ETS and FBI are generally confirmed also by other scores not shown, such as the Probability of Detection (POD) score or the False Alarm Rate (FAR).

As stated previously, higher skin SST Medspiration values affect precipitation magnitude. This outcome agrees with the average increase of upward moisture flux from the sea surface in domain D01 (+8% with GFS, +13% with IFS and IFS-DA in the 4-day time period). Vice versa (and contrary to what was found in the previous case study) the simulations do not show relevant differences in the timing of the event. If the accumulated values of average precipitation in each of the warning areas are considered, all simulations are very highly correlated (≥0.98, graph not shown) with observations. Fig. 13, showing the time series of hourly averaged water vapour flux through section BB', highlights that there are no relevant either forward or backward time deviations between the simulations with original skin SST fields and the corresponding simulations with Medspiration fields. The main effect observed in Fig. 13 is the lower flux of the GFS-based simulations because the main flow of soil moisture is shifted towards north-east with respect to the section BB' (in agreement with the precipitation maps in Fig. 11). The average flux increase with IFS-M and IFS-DA-M is of about 3-4%, vs. IFS-O and IFS-DA-O, respectively. Fig. 14, showing a snapshot of the IWV distribution in D01 during the event (31 October at 21:00 UTC), confirms the similar timing of the simulations. Moving from IFS-O to IFS-DA-O to IFS-DA-M, the size of the cluster of humid air south of Calabria increases, but its position is substantially the same. Similar conclusions are inferred from Fig. S6, providing additional information about 850 hPa wind fields in D02 at the same time of Fig. 14.

All simulations performed for this case study show that the greater energy supplied to the system by the higher skin SST Medspiration fields affects lower layers flow dynamics allowing more transport, but not accelerating it. This behaviour can be attributed to the long-lasting characteristics of the event that, developing at a wider scale than case study 1 and providing humid air continuously, smooths potential differences in terms of timing.

Assessing the hydrological impact in the two selected catchments is more interesting in this case study, because all simulations forecast heavy rain over the catchment areas of the Ancinale River and Bonamico Creek, yet it is still challenging because reliable hydrological forecasts require accurate QPFs at the catchment scale. A QPF performance analysis is carried out for the catchment areas, considering the average values of the interpolated precipitation fields. The simulated average precipitation over the Ancinale River catchment is strongly overestimated by all the IFS-based simulations in the 4-day forecasts (from +53% to +72%). Such overforecasts are only partially reduced to about +40% (except an increase to +80% with IFS-O) in the 3-day forecasts. GFS-based simulations provide much more reasonable biases in the 4-day forecasts (+12% and -1%, respectively for GFS-O and GFS-M), which are only partially confirmed in the 3-day forecasts, where GFS-M provides a nearly unbiased estimate (-3%) but GFS-O overforecast worsens to +44%. Concerning the Bonamico Creek catchment, in the 4-day forecasts the IFS-based biases are smaller in general (from -13% to +22%, but +54% with IFS-DA-M), while GFS-based simulations strongly underforecast (-56% and -43%, with GFS-O and GFS-M respectively). The 3-day bias is reduced for IFS-DA-based forecasts and slightly increased for IFS-based forecasts, with values however around -20% in all cases.

GFS-based forecasts are much improved (+10% and -16%, for GFS-O and GFS-M respectively). Taylor diagrams in Figs. 15a-d, based on the comparison of the average rainfall time series, generally show better performances of the GFS-based simulations in the Ancinale River and of the IFS-based simulations in the Bonamico Creek.

QPF analysis only partially reflects the main outcomes of the hydrological simulations, performed with the offline WRF-Hydro model forced with the WRF downscaled forecasts. According to precipitation overforecast of the IFS-based simulations, both Figs. 15e and 15g (4-day simulations) show a very relevant overestimation of all IFS-based hydrographs (except IFS-M in the Bonamico Creek). Nevertheless, in the case of the Ancinale River, IFS-O, IFS-M and IFS-DA-M hydrographs are reasonably correlated with observations (correlation coefficient *r* equal to 0.62, 0.77 and 0.70, respectively). Furthermore, simulated peak flow times of IFS-O and IFS-M hydrographs are very close to the observed occurring on 1 November 12 UTC (1 hour before and 4 hours after, respectively). The hydrographs resulting from GFS simulations are closer to observations in terms of volumes, nevertheless, peak times are significantly anticipated or delayed. Concerning the Bonamico Creek, IFS-based hydrographs are not well correlated and forecast peak flows more than 12 hours in advance compared to observations, while GFS-based hydrographs considerably underestimate.

The 3-day forecasts do not provide a substantial improvement. The hydrological simulations over the Ancinale River (Fig. 15f) are still affected by precipitation overforecasts. Furthermore, all simulations forecast the peak flows in advance compared to observations. Nevertheless, IFS-M, IFS-DA-O and IFS-DA-M show *r* values around 0.6. In particular, IFS-DA-O (highest *r*, equal to 0.65) forecasts the peak flow only 4 hours in advance. Despite the good performance with precipitation forecasts, GFS-M hydrograph is not well correlated with observations and simulates the observed peak flow about 9 hours in advance. With Bonamico Creek, IFS-DA-O results are even better (Fig. 15h). The simulated peak flow, according to precipitation forecasts, underestimates the observed of about 20%, but the correlation between simulated and observed hydrographs is high (0.89) and the observed peak flow time (1 November 16 UTC) is delayed by only 2 hours. Generally, all the IFS-based simulations are well correlated (*r* values always higher than 0.6) even though peak flow time is always delayed (up to 12 hours). GFS-based simulations are poorly correlated and show significant overestimation and early forecast of the peak flow.

4. DISCUSSIONS AND CONCLUSIONS

Table 5 aims at supporting the discussion summarizing the main outcomes concerning: 1) representation of the skin SST fields; 2) accumulated precipitation values in the internal domain and the related spatial distribution; 3) time distribution of precipitation and; 4) hydrological impact (hydrograph shape, total discharge, peak flow times), depending on 1) GCM choice for determining the boundary conditions; 2) use of the 3DVAR scheme; 3) use of the high-resolution Medspiration fields.

The most evident outcome across the case studies, yet far from surprising, is that the choice of the GCM providing boundary conditions is, comparatively, the most relevant factor affecting the simulations. Specifically, for the case studies analysed, GFS-based simulations are generally less performing than IFS-based (this difference is emphasized if the forecast time window is increased, such as case study 2 demonstrates). Of course, it is not a generalizable result, given the few events involved and

the lack of further analyses (e.g., evaluation of different parameterizations). For example, concerning case study 2, through detailed sensitivity tests, Avolio and Federico (2018) found that simulations forced by GFS have better performance than those forced by ECMWF. Nevertheless, for the purpose of this study it is shown that the different features differentiating the two GCMs (among that, the spatial resolution, which is improved with IFS) can considerably affect precipitation fields calculated through dynamical downscaling, comparatively more than using three-dimensional variational data assimilation methods or imposing specific (high-resolution) skin SST boundary conditions.

The use of the 3DVAR scheme in this study has to be considered mainly as a strategy for improving initial conditions. Several studies adopted data assimilation approaches for achieving improvements for forecast periods shorter than 48 to 96 hours used in this study (e.g., Sun et al., 2106; Gustafsson et al., 2018; Thiruvengadam et al., 2019), unless specific strategies were used (e.g., with cycling 3DVAR runs; Liu et al., 2018). Here, we focus on 2- to 4-day periods (depending on the case studies) for the sake of simplicity and clearness, testing the capability of different model configurations to reproduce the overall development of the hydrometeorological events, from their beginning to their end, checking also their usefulness in providing proper warning lead time. Therefore, testing extensively the 3DVAR scheme in order to get the highest benefit goes beyond the aims of this study.

Even though used with the underlined limitations, 3DVAR simulations provide some worthy outcomes. Concerning case study 1, applying the 3DVAR scheme with IFS boundary conditions results in a substantial increase of the average rainfall in the innermost domain (up to 25%), but this change does not provide clear advances in forecasting skills. That is consistent with previous studies, demonstrating that the effects of data assimilation do not lead to an effective improvement in the case of highly convective events (Liu et al., 2013). In case study 2 it is noteworthy that IFS-O is capable to provide in some warning areas, especially in the 4-day forecasts, better ETS values than IFS-DA-O, meaning that other sources of uncertainty than initial conditions can strongly affect forecasting skills. Among those uncertainties, representation of SST conditions can be important, given that, in general, IFS-DA-M (i.e., the simulation including both data assimilation and high-resolution SST representation) provides better performances.

Unlike the 3DVAR scheme, the effects of high-resolution SST representation on forecasts are emphasized to the maximum in this study, given that observed rather than forecasted SST fields are replaced as lower boundary conditions in the simulations, thereby providing a kind of "upper limit" to the effects provided by well forecasted SST fields. The foundation SST fields used (defined as the temperature of the water column, free of diurnal temperature variability, Donlon et al., 2007) are produced by the Medspiration project once every 24 hours, but the diurnal cycles are ensured by the *sst_skin* option. They especially improve the SST fields provided by IFS boundary conditions that, even allowing better forecasts than GFS, show very evident problems along the coastlines. The forecast periods analysed in this study allow to largely overcome the problem highlighted by Cassola et al. (2016), who found that for forecasting ranges shorter than 36-48 hours the forced ingestion of high-resolution SST fields can be counterproductive, due to the relatively slow adjustment of initial atmospheric fields.

High-resolution SST fields provide often, but not always (and not always significantly) enhanced forecast performances with respect to the corresponding simulations with native SST fields. Especially in case study 1, the effects close to the Corigliano

rain gauge seem to be somehow linked to generally chaotic behaviour. Such as discussed in the case of improved initial conditions (i.e., the 3DVAR scheme), these outcomes are related to the fact that other sources of uncertainties rather than SST representation hinder enhanced forecast skills. Furthermore, the average impact of high-resolution SST on the simulated precipitation in D02 is lower than expected with comprehensive approaches used to represent simulation uncertainty (e.g., ensemble forecast systems applied at convection-permitting resolutions; Evans et al., 2014). A preliminary analysis performed by the authors on case study 1 (not shown) using a convection-permitting ensemble system based on the ECMWF Ensemble Prediction System (EPS) highlights a mean absolute percentage deviation of about 24% for the perturbed simulations (against that found here, related to the SST fields resolution, equal to 4%).

Nevertheless, using more realistic SST fields leads to enough clear changes in the simulation of the atmospheric boundary layer dynamics in both case studies, especially with respect to the configurations with clearly unrealistic fields (i.e., IFS lower boundary conditions). Specifically, in the summer (shorter, convective, highly localized) event higher SST values along the coastlines accelerate flow dynamics, moving faster humid air towards the coast and moving up precipitation (thus agreeing with the results achieved by Stocchi and Davolio, 2017). On the other hand, in the autumn (longer, caused by a frontal system, widespread) event the higher energy supplied to the system by a continuously warmer sea surface leads to a generalized increase of precipitation amount that, however, does not change substantially either the spatial pattern or the timing of the event. The missed change in timing is most probably due to the fact that the stability of the atmospheric boundary layer and the related flow dynamics in case study 2 depend more on large scale (synoptic) conditions than local factors (that possibly is the same reason why, on the other hand, the 3DVAR scheme is capable to influence more case study 2 than case study 1). Such large-scale conditions are capable to lead to much stronger winds than case study 1 (that is evident comparing Figs. S3 and S6).

Exploring in detail the hydrological impact of case study 2, the analysis must be related to the resolution of the small-scale catchments, where the experiments show that results achieved on larger scales (i.e., at the resolution of the warning areas) can be ‘doubly’ reversed. For example, both bias analyses and Taylor diagrams related to the Ancinale River Basin (Figs. 15a-b) highlight better QPF performances for GFS-based simulations, not so obvious (or even not found) in the analysis of models skills on a larger scale. Nevertheless, IFS-based hydrographs are better correlated with those calculated with observed rainfall and peak flow times are closer to observed (it is worth to recall that a quantitative discharge analysis is less significant in this case, given that only water level observations are available). Contrary to what was found by Yucel et al. (2015), streamflow simulations are not particularly improved by initial data assimilation. Most probably, this result is due to the relatively long forecast periods (from 72 to 96 hours). Indeed, in the 3-day forecasts the benefits of the improved initial conditions partially come to light in both catchments even though, interestingly, the best simulation (even if only slightly) is IFS-DA-O, i.e. that using the 3DVAR scheme but not the Medspiration SST fields. Overall, the impact of reduced lead time from 4 to 3 days provides only slight enhancements (e.g., better performances of the GFS-based simulations or slightly higher ETS values), which however do not affect considerably the performance level of the hydrological forecasts.

Summarizing, the results achieved in this study show that none of the different versions of the forecasting chain adopted is capable to achieve in all the analysed cases quantitative precipitation and (consequently) streamflow forecast, yet several interesting clues are provided. Specifically, similar to past studies it is shown that the high-resolution representation of SST fields can significantly change the simulation of the atmospheric boundary layer processes, modifying flow dynamics and/or the amount of precipitated water. Nevertheless, the potentially positive impact of high-resolution SST fields can be easily hidden by several other sources of uncertainty (mainly, the relevance of the choice of the GCM providing boundary conditions). Further improvements in both GCMs (e.g., the higher-resolution IFS cycle since March 2016) and RCMs will reduce uncertainties highlighting more clearly the need for high-resolution SST representation in regional modelling. The topic of higher temporal frequency updating of lateral boundary conditions is also being actively investigated (Termonia et al., 2009; Matte et al., 2017; Keresturi et al., 2019). Furthermore, emerging approaches like regional-scale fully-coupled ocean-atmospheric (e.g., within the Baltic Sea Experiment – BALTEX, Gustafsson et al., 1998; Pullen et al., 2003; Ren et al., 2004; Loglisci et al., 2004; Ricchi et al., 2019; Lewis et al., 2019b) or ocean-atmospheric-hydrologic (Ruti et al.; 2016, Somot et al., 2018) modelling aim to directly calculate SST fields dynamics. Meanwhile, with the current generation of operational models, a reasonable (yet computationally demanding) solution is to adequately take into account the uncertainty of SST in forecasting chains adopting ensemble approaches also for this variable.

Data availability. Rainfall data are provided, upon request, by the "Centro Funzionale Multirischi – ARPACAL" (http://www.cfd.calabria.it/). Radar data are provided, upon request, by the Italian National Civil Protection "Centro Funzionale Centrale Rischio Meteo-idrogeologico e Idraulico" (http://www.protezionecivile.gov.it/home). Instruction for acquiring Medspiration L4 Ultra-High Resolution SSTfnd data are provided at http://cersat.ifremer.fr/thematic-portals/projects/medspiration. Observations used to perform data assimilation are available at https://rda.ucar.edu/. Simulation data are available from the corresponding author upon request.

Author contribution. All authors contributed equally to the manuscript.

Competing interests. The authors declare that they have no conflict of interest.

Acknowledgements. We thank the "Centro Funzionale Multirischi" of the Calabrian Regional Agency for the Protection of the Environment for providing the observed precipitation data and the Italian National Civil Protection "Centro Funzionale Centrale Rischio Meteo-idrogeologico e Idraulico" for providing radar data. L. Furnari acknowledges support from the Programme "POR Calabria FSE/FESR 2014/2020 – Mobilità internazionale di Dottorandi e Assegnisti di Ricerca/Ricercatori di Tipo A" Actions 10.5.6 and 10.5.12."

References

1. Allen, M., Frame, D., Kettleborough, J., and Stainforth, D.: Model error in weather and climate forecasting. In T. Palmer & R. Hagedorn (Eds.), Predictability of Weather and Climate (391-427). Cambridge: Cambridge University Press, https://doi.org/10.1017/CBO9780511617652.016, 2002.
2. Arnault, J., Wagner, S., Rummler, T., Fersch, B., Bliefernicht, J., Andresen, S., and Kunstmann, H.: Role of Runoff–Infiltration Partitioning and Resolved Overland Flow on Land–Atmosphere Feedbacks: A Case Study with the WRF-Hydro Coupled Modelling System for West Africa, J. Hydrometeor., 17, 1489–1516, https://doi.org/10.1175/JHM-D-15-0089.1, 2016.
3. Avolio, E., and Federico, S.: WRF simulations for a heavy rainfall event in southern Italy: Verification and sensitivity tests, Atmospheric Research, 209, 14-35. https://doi.org/10.1016/j.atmosres.2018.03.009, 2018.
4. Avolio, E., Cavalcanti, O., Furnari, L., Senatore, A., and Mendicino, G.: Brief communication: Preliminary hydro-meteorological analysis of the flash flood of 20 August 2018 in Raganello Gorge, southern Italy, Nat. Hazards Earth Syst. Sci., 19, 1619–1627, https://doi.org/10.5194/nhess-19-1619-2019, 2019.
5. Barker, D., Huang, X.-Y, Liu, Z., Auligné, T., Zhang, X., Rugg, S., Ajjaji, R., Bourgeois, A., Bray, J., Chen, Y., Demirtas, M., Guo, Y.-R, Henderson, T., Huang, W., Lin, H.-C., Michalakes, J., Rizvi, S., and Zhang, X.:The Weather Research and Forecasting Model's Community Variational/Ensemble Data Assimilation System: WRFDA, Bull. Amer. Meteor. Soc., 93, 831–843, https://doi.org/10.1175/BAMS-D-11-00167.1, 2012.
6. Barker, D.M., Huang, W., Guo, Y.R., Bourgeois, A.J., and Xiao., Q. N.: A Three-Dimensional (3DVAR) Data Assimilation System For Use With MM5: Implementation and Initial Results, Mon. Wea. Rev., 132, 897-914, https://doi.org/10.1175/1520-0493(2004)132<0897:ATVDAS>2.0.CO;2, 2004.
7. Berthou, S., Mailler, S., Drobinski, P., Arsouze, T., Bastin, S., Béranger, K., Flaounas, E., Lebeaupin Brossier, C., Somot, S., and Stéfanon, M.: Influence of submonthly air–sea coupling on heavy precipitation events in the Western Mediterranean basin, Q.J.R. Meteorol. Soc., 142, 453-471, https://doi.org/10.1002/qj.2717, 2016.
8. Berthou, S., Mailler, S., Drobinski, P., Arsouze, T., Bastin, S., Béranger, K., and Lebeaupin-Brossier, C.: Sensitivity of an intense rain event between atmosphere-only and atmosphere–ocean regional coupled models: 19 September 1996, Q.J.R. Meteorol. Soc., 141, 258-271,https://doi.org/10.1002/qj.2355, 2015.
9. Berthou, S., Mailler, S., Drobinski, P., Arsouze, T., Bastin, S., Béranger, K., and Lebeaupin-Brossier, C.: Prior history of Mistral and Tramontane winds modulates heavy precipitation events in southern France, Tellus A: Dynamic Meteorology and Oceanography, 66(1), 24064, https://doi.org/10.3402/tellusa.v66.24064, 2014.
10. Buizza, R.: Chapter 2 - Ensemble Forecasting and the Need for Calibration, Editor(s): Stéphane Vannitsem, Daniel S. Wilks, Jakob W. Messner, Statistical Postprocessing of Ensemble Forecasts, Elsevier, Pages 15-48, ISBN 9780128123720, https://doi.org/10.1016/B978-0-12-812372-0.00002-9, 2018.

11. Cabanes, C., Grouazel, A., von Schuckmann, K., Hamon, M., Turpin, V., Coatanoan, C., Paris, F., Guinehut, S., Boone, C., Ferry, N., de Boyer Montégut, C., Carval, T., Reverdin, G., Pouliquen, S., and Le Traon, P.-Y.: The CORA dataset: validation and diagnostics of in-situ ocean temperature and salinity measurements, Ocean Sci., 9, 1–18, https://doi.org/10.5194/os-9-1-2013, 2013.
12. Cassola, F., Ferrari, F., Mazzino, A., and Miglietta, M. M.: The role of the sea on the flash floods events over Liguria (northwestern Italy), Geophys. Res. Lett., 43, 3534– 3542, https://doi.org/10.1002/2016GL068265, 2016.
13. CFM (Centro Funzionale Multirischi della Calabria): Technical report, Rapporto speditivo di evento metopluviometrico del 12 agosto 2015 (in Italian)., available at http://www.cfd.calabria.it/DatiVari/Pubblicazioni/rapporto%20di%20evento%2012%20agosto.pdf (last access: 04 November 2019), 2015a.
14. CFM (Centro Funzionale Multirischi della Calabria): Technical report, Rapporto di evento metopluviometrico del 30 ottobre 2 novembre 2015 (in Italian)., available at http://www.cfd.calabria.it/DatiVari/Pubblicazioni/rapporto%20di%20evento%2030%20ottobre-2%20novembre2015.pdf (last access: 04 November 2019), 2015b.
15. Chen, S.H., and Sun, W-Y.: A One-dimensional Time Dependent Cloud Model, Journal of the Meteorological Society of Japan, 80(1), 99-118, https://doi.org/10.2151/jmsj.80.99, 2002.
16. Chiaravalloti, F., and Gabriele, S.: Vibo Valentia flood and MSG rainfall evaluation, Atmospheric Research, 93(1–3), 286-294,https://doi.org/10.1016/j.atmosres.2008.10.027, 2009.
17. Cohen, S., Praskievicz, S., and Maidment, D.R.: Featured Collection Introduction: National Water Model, Journal of the American Water Resources Association, 54(4), 767– 769. https://doi.org/10.1111/1752-1688.12664, 2018.
18. Cuo, L., Pagano, T.C., and Wang, Q.J.: A Review of Quantitative Precipitation Forecasts and Their Use in Short- to Medium-Range Streamflow Forecasting, J. Hydrometeor., 12, 713–728, https://doi.org/10.1175/2011JHM1347.1, 2011.
19. Davolio, S., Silvestro, F., and Gastaldo, T.: Impact of Rainfall Assimilation on High-Resolution Hydrometeorological Forecasts over Liguria, Italy, J. Hydrometeor., 18, 2659–2680, https://doi.org/10.1175/JHM-D-17-0073.1, 2017.
20. Davolio, S., Silvestro, F., and Malguzzi, P.: Effects of Increasing Horizontal Resolution in a Convection-Permitting Model on Flood Forecasting: The 2011 Dramatic Events in Liguria, Italy, J. Hydrometeor., 16, 1843–1856, https://doi.org/10.1175/JHM-D-14-0094.1, 2015.
21. Donlon, C., Robinson, I., Casey, K.S., Vazquez-Cuervo, J., Armstrong, E., Arino, O., Gentemann, C., May, D., LeBorgne, P., Piollé, J., Barton, I., Beggs, H., Poulter, D.J., Merchant, C.J., Bingham, A., Heinz, S., Harris, A., Wick, G., Emery, B., Minnett, P., Evans, R., Llewellyn-Jones, D., Mutlow, C., Reynolds, R.W., Kawamura, H., and Rayner, N.: The Global Ocean Data Assimilation Experiment High-resolution Sea Surface Temperature Pilot Project, Bull. Amer. Meteor. Soc., 88, 1197–1214, https://doi.org/10.1175/BAMS-88-8-1197, 2007.

22. Drobinski, P., Silva, N.D., Panthou, G., Bastin, S., Muller, C., Ahrens, B., Borga, B., Conte, D., Fosser, G., Giorgi, F., Güttler, I., Kotroni, V., Li, L., Morin, E., Önol, B., Quintana-Segui, P., Romera, R., and Torma, C. S.: Scaling precipitation extremes with temperature in the Mediterranean: past climate assessment and projection in anthropogenic scenarios, Clim. Dyn., 51, 1237-1257, https://doi.org/10.1007/s00382-016-3083-x, 2018.
23. Dudhia, J.: Numerical Study of Convection Observed during the Winter Monsoon Experiment Using a Mesoscale Two-Dimensional Model, J. Atmos. Sci., 46, 3077–3107, https://doi.org/10.1175/1520-0469(1989)046<3077:NSOCOD>2.0.CO;2, 1989.
24. Evans, C., Dyke, D., and Lericos, T.: How Do Forecasters Utilize Output from a Convection-Permitting Ensemble Forecast System? Case Study of a High-Impact Precipitation Event, Weather and Forecasting, 29, 466–486, https://doi.org/10.1175/WAF-D-13-00064.1, 2014.
25. Federico, S., Avolio, E., Bellecci, C., Lavagnini, A., Colacino, M., and Walko, R. L.: Numerical analysis of an intense rainstorm occurred in southern Italy, Nat. Hazards Earth Syst. Sci., 8, 19-35, https://doi.org/10.5194/nhess-8-19-2008, 2008.
26. Federico, S., Bellecci, C., and Colacino, M.: Numerical simulation of Crotone flood: storm evolution. Il Nuovo Cimento C. 26C, 357–371, 2003a.
27. Federico, S., Bellecci, C., and Colacino, M.: Quantitative precipitation of the Soverato flood: the role of orography and surface fluxes. Il Nuovo Cimento C. 26 C, 7–22, 2003b.
28. Federico, S., Pasqualoni, L., Avolio, E., and Bellecci, C.: Brief communication "Calabria daily rainfall from 1970 to 2006", Nat. Hazards Earth Syst. Sci., 10, 717-722, https://doi.org/10.5194/nhess-10-717-2010 , 2010.
29. Gascón, E., Laviola, S., Merino, A., and Miglietta, M.M.: Analysis of a localized flash-flood event over the central Mediterranean, Atmospheric Research, 182, 256-268, https://doi.org/10.1016/j.atmosres.2016.08.007, 2016.
30. Gochis, D.J., Yu, W. and Yates, D.: The WRF-Hydro model technical description and user's guide, version 3.0. NCAR Tech. Doc. 120. https://doi.org/10.5065/D6DN43TQ, 2015.
31. Gronewold, A.D., Clites, A.H., Hunter, T.S., and Stow, C.G.: An appraisal of the Great Lakes advanced hydrologic prediction system, Journal of Great Lakes Research, 37 (3), 577-583, https://doi.org/10.1016/j.jglr.2011.06.010, 2011.
32. Gustafsson, N., Nyberg, L., and Omstedt, A.: Coupling of a High-Resolution Atmospheric Model and an Ocean Model for the Baltic Sea, Monthly Weather Review, 126, 2822-2846, https://doi.org/10.1175/1520-0493(1998)126<2822:COAHRA>2.0.CO;2, 1998.
33. Gustafsson, N, Janjić, T, Schraff, C, Leuenberger, D., Weissmann, M., Reich, H., Brousseau, P., Montmerle, T., Wattrelot, E., Bučánek, A., Mile, M., Hamdi, R., Lindskog, M., Barkmeijer, J., Dahlbom, M., Macpherson, B., Ballard, S., Inverarity, G., Carley, J., Alexander, C., Dowell, D., Liu, S., Ikuta, Y., and Fujita, T.: Survey of data assimilation methods for convective-scale numerical weather prediction at operational centres. Q.J.R. Meteorol Soc., 144, 1218– 1256. https://doi.org/10.1002/qj.3179, 2018.

34. Hodur, R.M.: The Naval Research Laboratory's Coupled Ocean/Atmosphere Mesoscale Prediction System (COAMPS). Mon. Wea. Rev., 125, 1414–1430, https://doi.org/10.1175/1520-0493(1997)125<1414:TNRLSC>2.0.CO;2, 1997.

35. Huang, X.Y., Xiao, Q., Barker, D.M., Zhang, X., Michalakes, J., Huang, W., Henderson, T., Bray, J., Chen, Y., Ma, Z., Dudhia, J., Guo, Y., Zhang, X., Won, D.J., Lin, H.C., and Kuo, Y.H.: Four-Dimensional Variational Data Assimilation for WRF: Formulation and Preliminary Results, Mon. Wea. Rev., 137, 299–314, https://doi.org/10.1175/2008MWR2577.1, 2009.

36. Hydrologic Engineering Center, HEC-RAS, River Analysis System, Hydraulic Reference Manual. Version 5.0, U.S. Army Corps of Engineers, Davis, California, 2016.

37. Ivatek-Šahdan, Stanešić, S.A., Tudor, M., Plenković, I.O., and Janeković, I.: Impact of SST on heavy rainfall events on eastern Adriatic during SOP1 of HyMeX, Atmospheric Research, 200, 36-59https://doi.org/10.1016/j.atmosres.2017.09.019, 2018.

38. Janjić, Z.I.: The Step-Mountain Eta Coordinate Model: Further Developments of the Convection, Viscous Sublayer, and Turbulence Closure Schemes, Mon. Wea. Rev., 122, 927–945, https://doi.org/10.1175/1520-0493(1994)122<0927:TSMECM>2.0.CO;2, 1994.

39. Jansa, A., Alpert, P., Arbogast, P., Buzzi, A., Ivancan-Picek, B., Kotroni, V., Llasat, M. C., Ramis, C., Richard, E., Romero, R., and Speranza, A.: MEDEX: a general overview, Nat. Hazards Earth Syst. Sci., 14, 1965-1984, https://doi.org/10.5194/nhess-14-1965-2014, 2014.

40. Kain, J.S.: The Kain–Fritsch Convective Parameterization: An Update, J. Appl. Meteor., 43, 170–181, https://doi.org/10.1175/1520-0450(2004)043<0170:TKCPAU>2.0.CO;2, 2004.

41. Katsafados, P., Mavromatidis, E., Papadopoulos, A., and Pytharoulis, I.: Numerical simulation of a deep Mediterranean storm and its sensitivity on sea surface temperature, Nat. Hazards Earth Syst. Sci., 11, 1233-1246, https://doi.org/10.5194/nhess-11-1233-2011 , 2011.

42. Keresturi, E., Wang, Y., Meier, F., Weidle, F., and Wittman, C.: Improving initial condition perturbations in a convection-permitting ensemble prediction system, Quarterly Journal of the Royal Meteorological Society, 145, 993-1012, https://doi.org/10.1002/qj.3473, 2019.

43. Lahmers, T.M., Gupta, H., Castro, C.L., Gochis, D.J., Yates, D., Dugger, A., Goodrich, D., and Hazenberg, P.: Enhancing the Structure of the WRF-Hydro Hydrologic Model for Semiarid Environments, J. Hydrometeor., 20, 691–714, https://doi.org/10.1175/JHM-D-18-0064.1, 2019.

44. Lebeaupin, C., Ducrocq, V., and Giordani, H.: Sensitivity of torrential rain events to the sea surface temperature based on high-resolution numerical forecasts, J. Geophys. Res., 111, D12110, https://doi.org/10.1029/2005JD006541, 2006.

45. Lewis, H. W., Castillo Sanchez, J. M., Arnold, A., Fallmann, J., Saulter, A., Graham, J., Bush, M., Siddorn, J., Palmer, T., Lock, A., Edwards, J., Bricheno, L., Martínez-de la Torre, A., and Clark, J.: The UKC3 regional coupled

environmental prediction system, Geosci. Model Dev., 12, 2357–2400, https://doi.org/10.5194/gmd-12-2357-2019, 2019a.

46. Lewis, H. W., Siddorn, J., Castillo Sanchez, J. M., Petch, J., Edwards, J. M., and Smyth, T.: Evaluating the impact of atmospheric forcing and air–sea coupling on near-coastal regional ocean prediction, Ocean Sci., 15, 761-778, https://doi.org/10.5194/os-15-761-2019, 2019b.
47. Li, J., Chen, Y., Wang, H., Qin, J., Li, J., and Chiao, S.: Extending flood forecasting lead time in a large watershed by coupling WRF QPF with a distributed hydrological model, Hydrol. Earth Syst. Sci., 21, 1279-1294, https://doi.org/10.5194/hess-21-1279-2017 , 2017.
48. Lin, P., Yang, Z.-L. Gochis, D.J., Yu, W., Maidment, D.R., Somos-Valenzuela, M.A., and David, C.H.: Implementation of a vector-based river network routing scheme in the community WRF-Hydro modelling framework for flood discharge simulation, Environmental Modelling & Software, 107, 1-11, https://doi.org/10.1016/j.envsoft.2018.05.018, 2018.
49. Liu, J., Bray, M., and Han, D.: Exploring the effect of data assimilation by WRF-3DVar for numerical rainfall prediction with different types of storm events, Hydrol. Process., 27, 3627-3640. https://doi.org/10.1002/hyp.9488, 2013.
50. Liu, J., Tian, J., Yan, D., Li, C., Yu, F., and Shen, F.: Evaluation of Doppler radar and GTS data assimilation for NWP rainfall prediction of an extreme summer storm in northern China: from the hydrological perspective, Hydrol. Earth Syst. Sci., 22, 4329-4348, https://doi.org/10.5194/hess-22-4329-2018, 2018.
51. Liu, Y., Weerts, A. H., Clark, M., Hendricks Franssen, H.-J., Kumar, S., Moradkhani, H., Seo, D.-J., Schwanenberg, D., Smith, P., van Dijk, A. I. J. M., van Velzen, N., He, M., Lee, H., Noh, S. J., Rakovec, O., and Restrepo, P.: Advancing data assimilation in operational hydrologic forecasting: progresses, challenges, and emerging opportunities, Hydrol. Earth Syst. Sci., 16, 3863-3887, https://doi.org/10.5194/hess-16-3863-2012 , 2012.
52. Llasat, M. C., Llasat-Botija, M., Petrucci, O., Pasqua, A. A., Rosselló, J., Vinet, F., and Boissier, L.: Towards a database on societal impact of Mediterranean floods within the framework of the HYMEX project, Nat. Hazards Earth Syst. Sci., 13, 1337-1350, https://doi.org/10.5194/nhess-13-1337-2013 , 2013.
53. Loglisci, N., Qian, M. W., Rachev, N., Cassardo, C., Longhetto, A., Purini, R., Trivero, P., Ferrarese, S., and Giraud, C.: Development of an atmosphere-ocean coupled model and its application over the Adriatic Sea during a severe weather event of Bora wind, J. Geophys. Res., 109, D01102, https://doi.org/10.1029/2003JD003956, 2004.
54. Manzato, A., Davolio, S., Miglietta, M. M., Pucillo, A., and Setvák, M.: 12 September 2012: A supercell outbreak in NE Italy?, Atmospheric Research, 153, 98-118, https://doi.org/10.1016/j.atmosres.2014.07.019, 2015.
55. Matte, D., Laprise, R., Thériault, J.M., and Lucs-Picher, P.: Spatial spin-up of fine scales in a regional climate model simulation driven by low-resolution boundary conditions, Clim. Dyn., 49, 563-574, https://doi.org/10.1007/s00382-016-3358-2, 2017.

56. Mellor, G. L., and Yamada, T.: Development of a turbulence closure model for geophysical fluid problems, Rev. Geophys., 20(4), 851– 875, https://doi.org/10.1029/RG020i004p00851, 1982.
57. Merchant, C. J., Filipiak, M. J., Le Borgne, P., Roquet, H., Autret, E., Piolle, J.F., and Lavender, S.: Diurnal warm-layer events in the western Mediterranean and European shelf seas, Geophysical Research Letters, 35(L04601), 1-4, http://dx.doi.org/10.1029/2007GL033071, 2008.
58. Meredith, E.P., Maraun, D., Semenov, V.A., and Park, W.: Evidence for added value of convection-permitting models for studying changes in extreme precipitation, J. Geophys. Res. Atmos., 120, 12500– 12513, https://doi.org/10.1002/2015JD024238, 2015.
59. Miglietta, M.M., Bueso, J., Motola, V., and Pasini, A.: Effect of a positive Sea Surface Temperature anomaly on a Mediterranean tornadic supercell, Scientific Reports, 7, 12828, https://doi.org/10.1038/s41598-017-13170-0, 2017.
60. Miglietta, M.M., Moscatello, A., Conte, D., Mannarini, G., Lacorata, G., and Rotunno R.: Numerical analysis of a Mediterranean 'hurricane' over south-eastern Italy: Sensitivity experiments to sea surface temperature, Atmospheric Research, 101(1-2) 412-426, https://doi.org/10.1016/j.atmosres.2011.04.006, 2011.
61. Mlawer, E. J., Taubman, S. J., Brown, P. D., Iacono, M. J., and Clough, S. A.: Radiative transfer for inhomogeneous atmospheres: RRTM, a validated correlated-k model for the longwave, J. Geophys. Res., 102(D14), 16663– 16682, https://doi.org/10.1029/97JD00237, 1997.
62. Pagano, T. C., Wood, A.W., Ramos, M.H., Cloke, H.L., Pappenberger, F., Clark, M.P., Cranston, M., Kavetski, D., Mathevet, T., Sorooshian, S., and Verkade, J.S.: Challenges of operational river forecasting, Journal of Hydrometeorology, 15,1692-1707., https://doi.org/10.1175/JHM-D-13-0188.1 , 2014.
63. Pastor, F., Valiente, J. A., and Estrela, M. J.: Sea surface temperature and torrential rains in the Valencia region: modelling the role of recharge areas, Nat. Hazards Earth Syst. Sci., 15, 1677-1693, https://doi.org/10.5194/nhess-15-1677-2015, 2015.
64. Petrucci, O., Salvati, P., Aceto, L., Bianchi, C., Pasqua, A.A., Rossi, M., and Guzzetti, F.: The Vulnerability of People to Damaging Hydrogeological Events in the Calabria Region (Southern Italy). Int. J. Environ. Res. Public Health, 15(1), 48, https://doi.org/10.3390/ijerph15010048, 2018.
65. Pullen, J., Doyle, J. D., Hodur, R., Ogston, A., Book, J. W., Perkins, H., and Signell, R.: Coupled ocean-atmosphere nested modelling of the Adriatic Sea during winter and spring 2001, J. Geophys. Res., 108, 3320, https://doi.org/10.1029/2003JC001780, 2003.
66. Pytharoulis, I.: Analysis of a Mediterranean tropical-like cyclone and its sensitivity to the sea surface temperatures, Atmospheric Research, 208, 167-179, https://doi.org/10.1016/j.atmosres.2017.08.009, 2018.
67. Rainaud, R., Lebeaupin Brossier, C., Ducrocq, V., Giordani, H., Nuret, M., Fourrié, N., Bouin, M., Taupier-Letage, I., and Legain, D.: Characterization of air–sea exchanges over the Western Mediterranean Sea during HyMeX SOP1 using the AROME–WMED model, Q.J.R. Meteorol. Soc., 142, 173-187, https://doi.org/10.1002/qj.2480 , 2016.

68. Ren, X., Perrie, W., Long, Z. and Gyakum, J.: Atmosphere–Ocean Coupled Dynamics of Cyclones in the Midlatitudes, Mon. Wea. Rev., 132, 2432–2451, https://doi.org/10.1175/1520-0493(2004)132<2432:ACDOCI>2.0.CO;2 , 2004.

69. Renard, B., Kavetski, D., Kuczera, G., Thyer, M., and Franks, S. W.: Understanding predictive uncertainty in hydrologic modelling: The challenge of identifying input and structural errors, Water Resour. Res., 46, W05521, https://doi.org/10.1029/2009WR008328, 2010.

70. Ricchi, A., Miglietta, M.M., Bonaldo, D., Cioni, G., Rizza, U., and Carniel, S.: Multi-Physics Ensemble versus Atmosphere–Ocean Coupled Model Simulations for a Tropical-Like Cyclone in the Mediterranean Sea, Atmosphere, 10, 202, https://doi.org/10.3390/atmos10040202, 2019.

71. Robinson, I., Piolle, J.F., Leborgne, P., Poulter, D., Donlon, C., and Arino, O.: Widening the application of AATSR SST data to operational tasks through the Medspiration Service, Remote Sensing Of Environment, 116, 126-139: http://dx.doi.org/10.1016/j.rse.2010.12.019, 2012.

72. Romaniello, V., Oddo, P., Tonani, M., Torrisi, L., Grandi, A., and Pinardi, N.: Impact of Sea Surface Temperature on COSMO Forecasts of a Medicane over the Western Mediterranean Sea, Journal of earth science and engineering, 5, 338-348, https://doi.org/10.17265/2159-581X/2015.06.002, 2015.

73. Ruti, P.M., Somot, S., Giorgi, F., Dubois, C., Flaounas, E., Obermann, A., Dell'Aquila, A., Pisacane, G., Harzallah, A., Lombardi, E., Ahrens, B., Akhtar, N., Alias, A., Arsouze, T., Aznar, R., Bastin, S., Bartholy, J., Béranger, K., Beuvier, J., Bouffies-Cloché, S., Brauch, J., Cabos, W., Calmanti, S., Calvet, J., Carillo, A., Conte, D., Coppola, E., Djurdjevic, V., Drobinski, P., Elizalde-Arellano, A., Gaertner, M., Galàn, P., Gallardo, C., Gualdi, S., Goncalves, M., Jorba, O., Jordà, G., L'Heveder, B., Lebeaupin-Brossier, C., Li, L., Liguori, G., Lionello, P., Maciàs, D., Nabat, P., Önol, B., Raikovic, B., Ramage, K., Sevault, F., Sannino, G., Struglia, M.V., Sanna, A., Torma, C. and Vervatis, V.: Med-CORDEX Initiative for Mediterranean Climate Studies, Bull. Amer. Meteor. Soc., 97, 1187–1208, https://doi.org/10.1175/BAMS-D-14-00176.1 , 2016.

74. Salas, F.R., Somos-Valenzuela, M.A., Dugger, A., Maidment, D.R., Gochis, D.J., David, C. H., Yu, W., Ding, D., Clark, E.P., and Noman, N.: Towards Real-Time Continental Scale Streamflow Simulation in Continuous and Discrete Space, Journal of the American Water Resources Association (JAWRA) 54(1), 7- 27, https://doi.org/10.1111/1752-1688.12586, 2018.

75. Senatore, A., Mendicino, G., Gochis, D. J., Yu, W., Yates, D. N., and Kunstmann, H.: Fully coupled atmosphere-hydrology simulations for the central Mediterranean: Impact of enhanced hydrological parameterization for short and long time scales, J. Adv. Model. Earth Syst., 7, 1693– 1715, https://doi.org/10.1002/2015MS000510, 2015.

76. Senatore, A., Mendicino, G., Knoche, H.R. and Kunstmann, H.: Sensitivity of Modelled Precipitation to Sea Surface Temperature in Regions with Complex Topography and Coastlines: A Case Study for the Mediterranean, J. Hydrometeor., 15, 2370–2396, https://doi.org/10.1175/JHM-D-13-089.1, 2014.

77. Silvestro, F., Rebora, N., Cummings, G. and Ferraris, L.: Dealing with flash floods using a hydrological nowcasting chain. J. Flood Risk Manage, 10, 446-462. https://doi.org/10.1111/jfr3.12161, 2017.
78. Sinclair, S. and Pegram, G.: Combining radar and rain gauge rainfall estimates using conditional merging, Atmosph. Sci. Lett., 6, 19-22, https://doi.org/10.1002/asl.85, 2005.
79. Skamarock, W. C., Klemp, J.B., Dudhia, J., Gill, D. O., Barker, D. M., Duda, M. G., Huang, X.-Y., Wang, W., and Powers, J.G.: A Description of the Advanced Research WRF Version 3. *NCAR Tech. Note NCAR/TN-475+STR*, 113 pp. https://doi.org/10.5065/D68S4MVH, 2008.
80. Somot, S., Ruti, P., Ahrens, B. Coppola, E., Jordà G., Sannino, G., and Solmon F.: Editorial for the Med-CORDEX special issue, Clim. Dyn., 51, 771-777, https://doi.org/10.1007/s00382-018-4325-x, 2018.
81. Stocchi, P., and Davolio, S.: Intense air-sea exchanges and heavy orographic precipitation over Italy: The role of Adriatic sea surface temperature uncertainty, Atmospheric Research, 196, 62-82, https://doi.org/10.1016/j.atmosres.2017.06.004, 2017.
82. Sun, J., Wang, H., Tong, W., Zhang, Y., Lin, C., and Xu, D.: Comparison of the Impacts of Momentum Control Variables on High-Resolution Variational Data Assimilation and Precipitation Forecasting, Mon. Wea. Rev., 144, 149–169, https://doi.org/10.1175/MWR-D-14-00205.1, 2016.
83. Tao, J., Wu, D., Gourley, J., Zhang, S.Q., Crow, W., Peters-Lidard, C., and Barros A.P.: Operational hydrological forecasting during the IPHEx-IOP campaign – Meet the challenge, Journal of Hydrology, Volume 541, Part A, 434-456, https://doi.org/10.1016/j.jhydrol.2016.02.019, 2016.
84. Termonia, P., Deckmyn, A., and Hamdi, R.: Study of the lateral boundary condition temporal resolution problem and a proposed solution by means of boundary error restarts. Mon. Weather Rev., 137, 3551–3566, https://doi.org/10.1175/2009MWR2964.1, 2009.
85. Tewari, M., Chen, F., Wang, W., Dudhia, J., LeMone, M.A., Mitchell, K., Ek, M., Gayno, G., Wegiel, J., and Cuenca, R.H.: Implementation and verification of the unified NOAH land surface model in the WRF model. 20th conference on weather analysis and forecasting/16th conference on numerical weather prediction, pp. 11–15, 2004.
86. Thiruvengadam, P., Indu, J., and Ghosh, S.: Assimilation of Doppler Weather Radar data with a regional WRF-3DVAR system: Impact of control variables on forecasts of a heavy rainfall case, Advances in Water Resources, 126, 24-39, https://doi.org/10.1016/j.advwatres.2019.02.004, 2019.
87. Verri, G., Pinardi, N., Gochis, D., Tribbia, J., Navarra, A., Coppini, G., and Vukicevic, T.: A meteo-hydrological modelling system for the reconstruction of river runoff: the case of the Ofanto river catchment, Nat. Hazards Earth Syst. Sci., 17, 1741-1761, https://doi.org/10.5194/nhess-17-1741-2017, 2017.
88. Wilks, S.D.: Statistical Methods in the Atmospheric Sciences. International Geophysics Series, 59, https://doi.org/10.1016/S0074-6142(06)80036-7, 2006.

89. Yucel, I., Onen, A., Yilmaz, K. and Gochis, D. J.: Calibration and Evaluation of a Flood Forecasting System: Utility of Numerical Weather Prediction Model, Data Assimilation and Satellite-Based Rainfall. Journal of Hydrology, 523, 49-66, https://doi.org/10.1016/j.jhydrol.2015.01.042, 2015.

90. Zeng, X., and Beljaars, A.: A prognostic scheme of sea surface skin temperature for modelling and data assimilation. Geophysical Research Letters 32, L14605. https://doi.org/10.1029/2005GL023030, 2005.

Figures

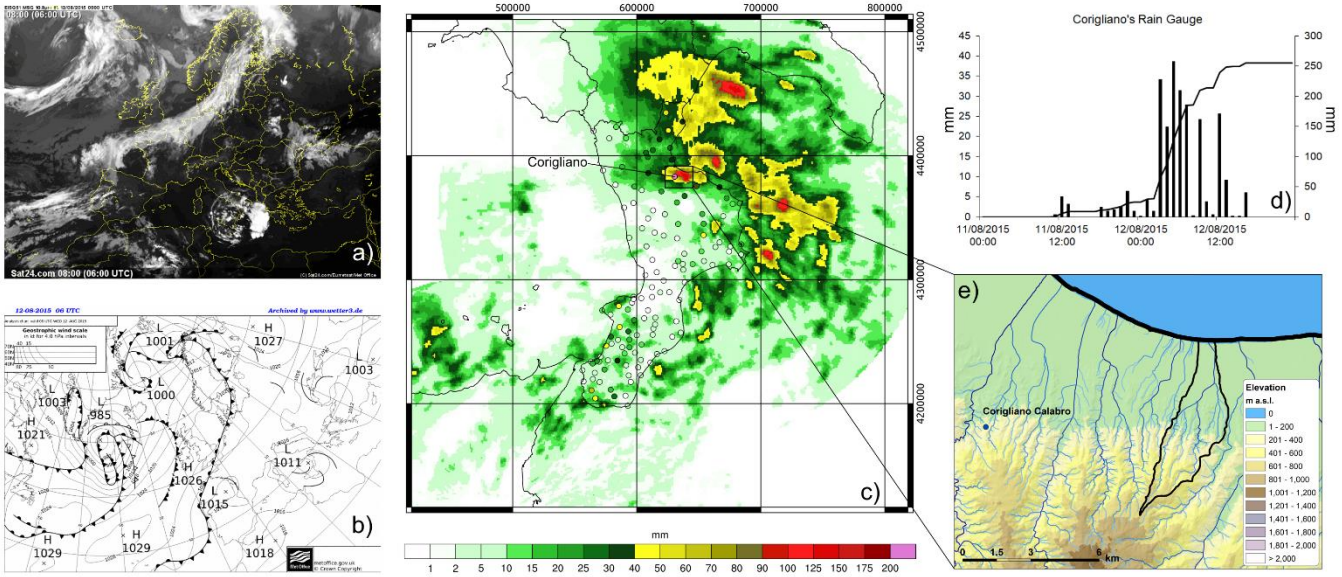

Fig. 1. a) satellite images of the thermal infrared channel (10.8 µm) at 06 UTC 12 August 2015, source: www.sat24.com, ©Eumetsat; b) surface pressure and weather fronts at 06 UTC 12 August 2015, source: www.wetter3.de, @Metoffice; c) cumulative rain (mm) observed between 18 UTC 11 August 2015 and 18 UTC 12 August 2015, points represent the weather stations while spatially distributed values represent the radar estimation; d) cumulative and hourly rainfall (mm) observed at the Corigliano rain gauge; e) the Citrea Creek catchment with the Corigliano rain gauge.

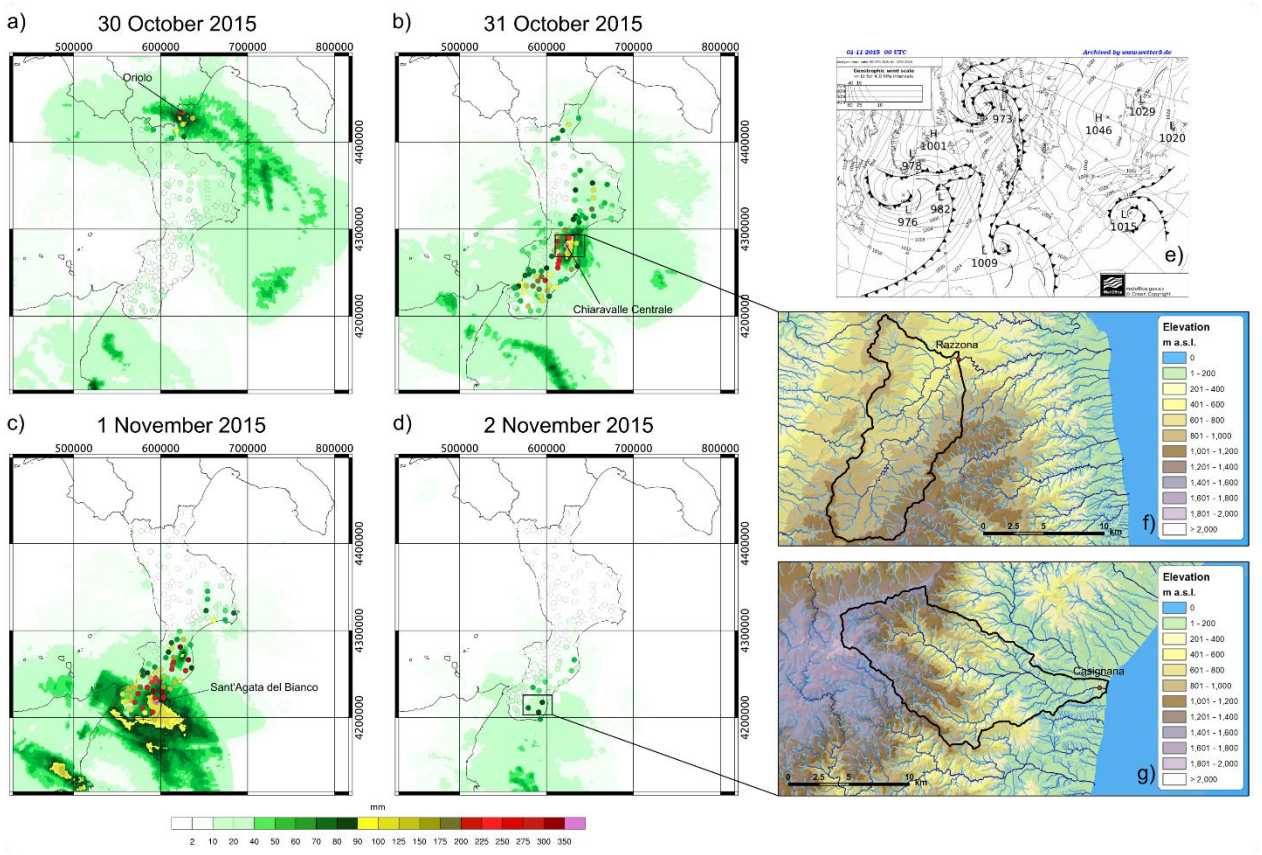

Fig. 2. From a) to d): daily rainfall (mm) observed from 30 October 2015 to 2 November 2015, points represent the weather stations while spatially distributed values represent the radar estimation; e) surface pressure and weather fronts at 00 UTC 1 November 2015, source www.wetter3.de, @Metoffice; f) Ancinale River catchment; g) Bonamico Creek catchment.

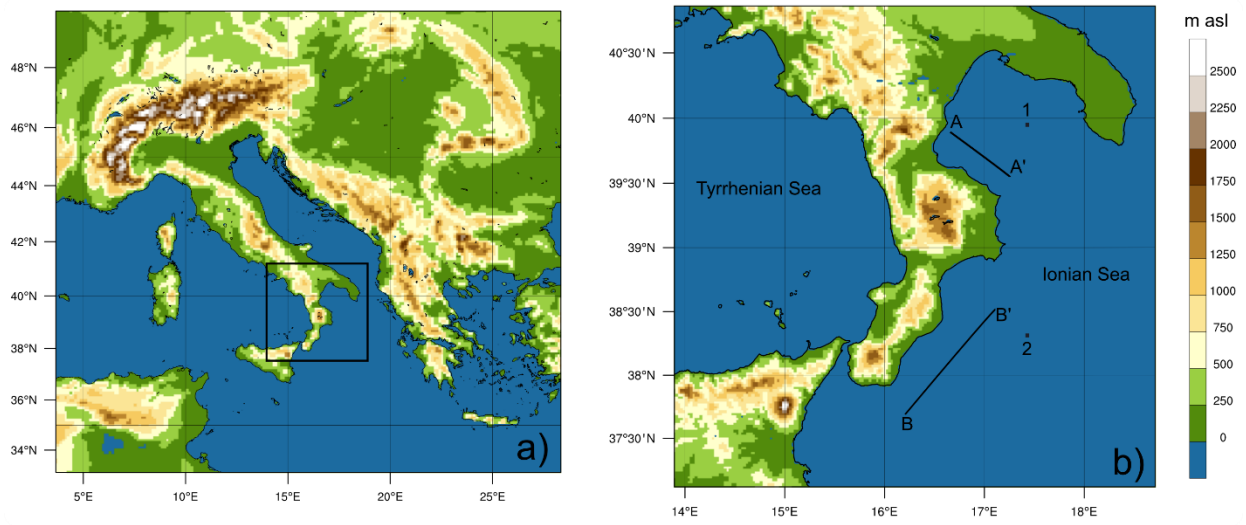

Fig. 3. a) outer domain (D01) with a spatial resolution of 10 km; b) inner domain (D02) with a spatial resolution of 2 km. Points 1 and 2 are considered for evaluating SSTSK evolution locally during the events according to different configurations (Fig. 5 and Fig. 10, respectively). Across sections A-A' and B-B' vertically integrated water vapour fluxes are calculated (Fig. 9 and Fig. 13, respectively).

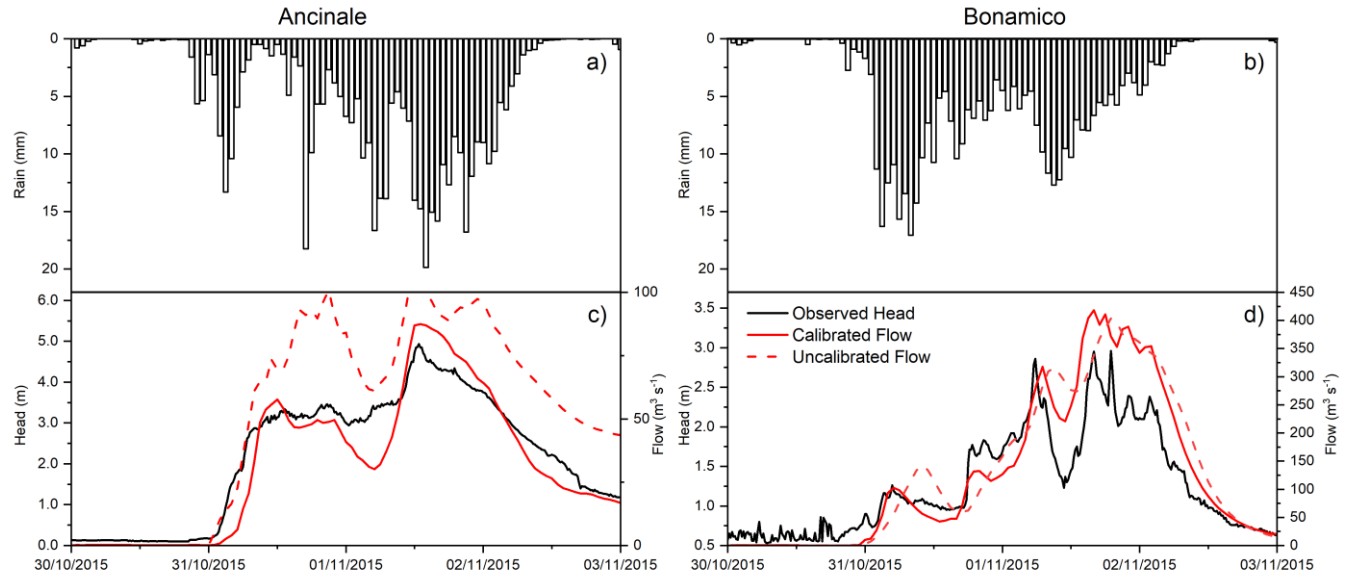

Fig. 4. a) Observed hourly rainfall (mm) averaged over the Ancinale River catchment; b) as a), but for the Bonamico Creek catchment; c) comparison between observed hydrometric levels (m), uncalibrated and calibrated simulated flow ($m^3 s^{-1}$) over the Ancinale River catchment; d) as c), but for the Bonamico Creek catchment.

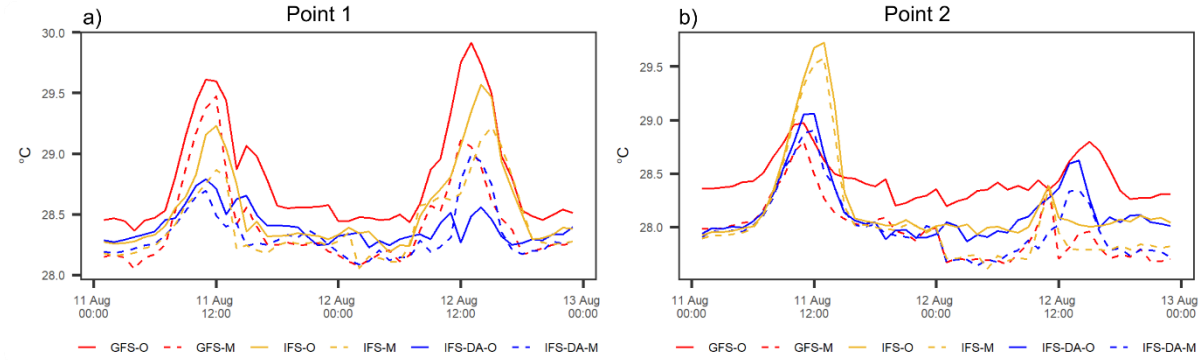

Fig. 5. Case study 1: temporal evolution of SSTSK (°C) at points 1 and 2 highlighted in Fig. 3b.

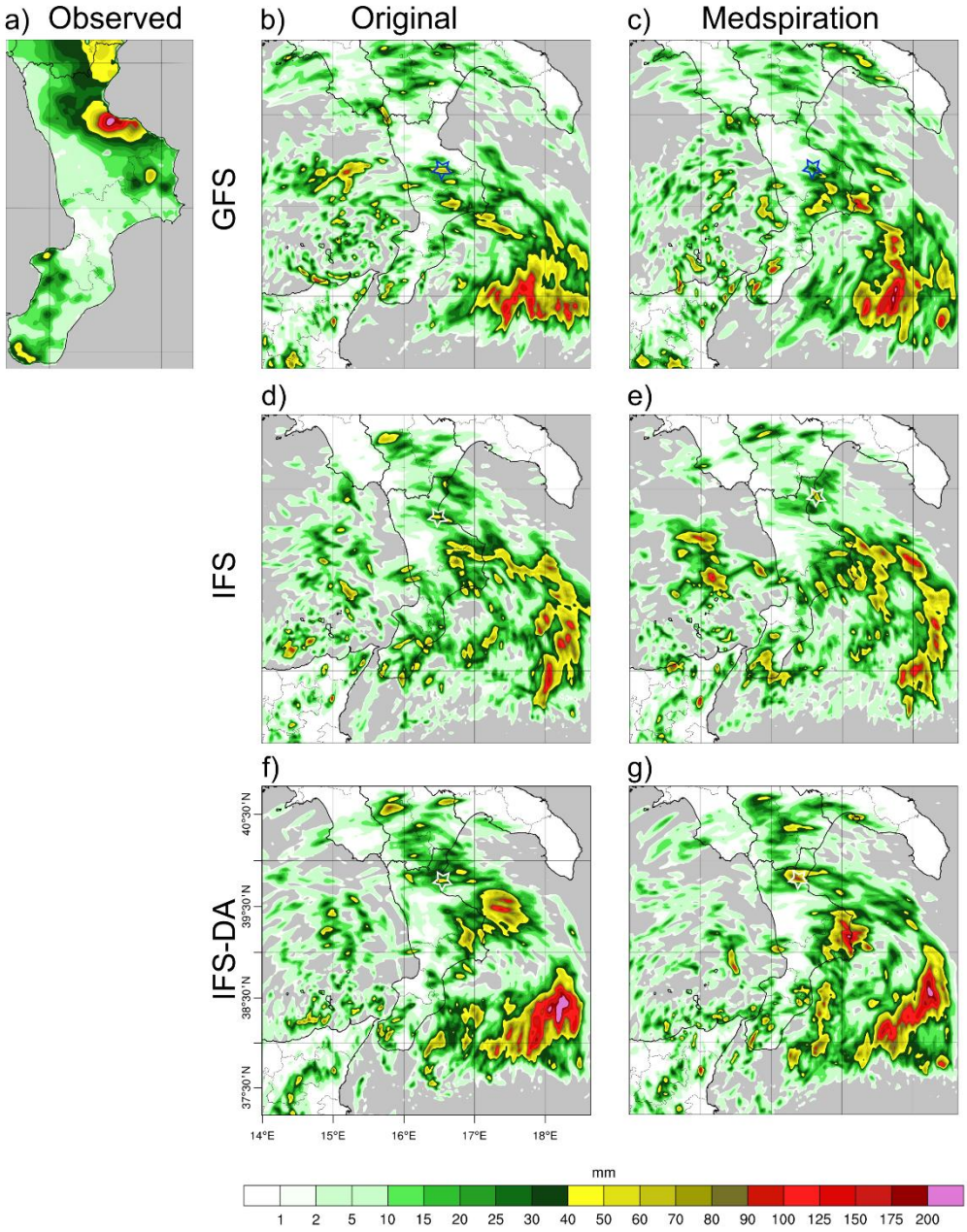

Fig. 6. 24-hours accumulated precipitation (mm) from 18 UTC 11 August 2015 to 18 UTC 12 August 2015: a) merged ground measurements and radar observations and simulated (b-g) with different configurations. The small blue (Figs. 6b-c) or white (Figs. 6d-g) stars highlight the accumulated rainfall peaks near Corigliano analysed in detail in Fig. 7.

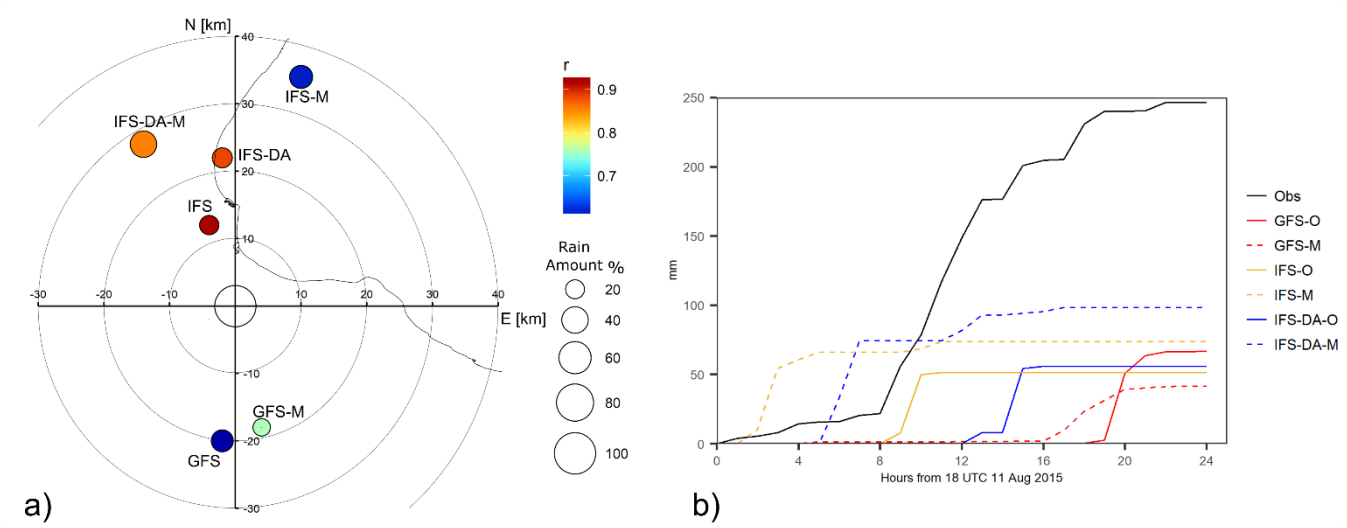

Fig. 7. Circles in a) are located at the peaks highlighted in Fig. 6 for each of the different configurations; the colours indicate the time correlation, while the size refers to the percentage rain amount with respect to Corigliano observations; b) temporal accumulated rainfall (mm) observed at Corigliano and simulated by the different peaks.

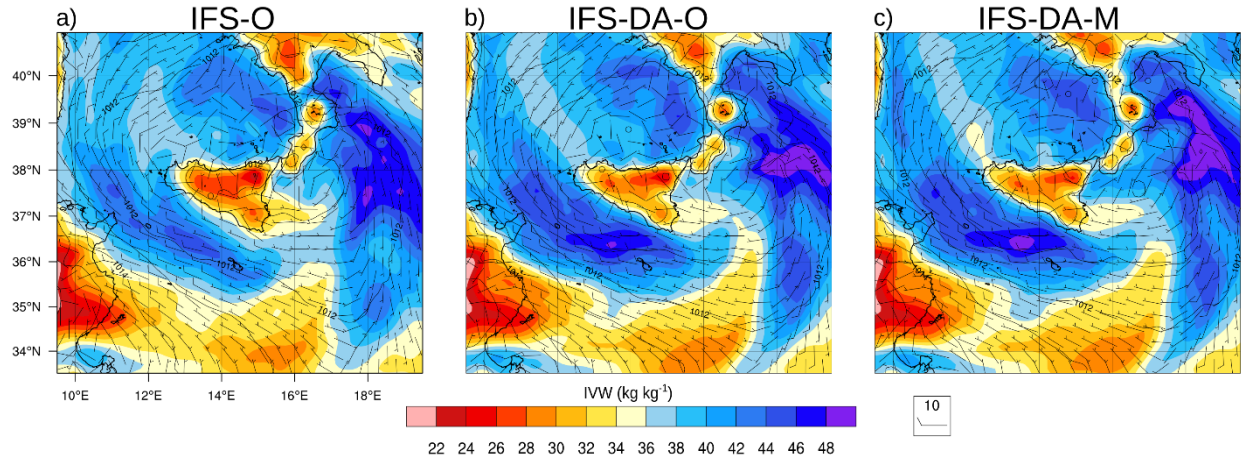

Fig. 8. Column IWV (kg kg^{-1}, colour), sea level pressure (hPa; contours), wind direction and speed (barbs) at 10m height at 03 UTC 12 August 2015 for a) IFS-O; b) IFS-DA-O and c) IFS-DA-M, respectively.

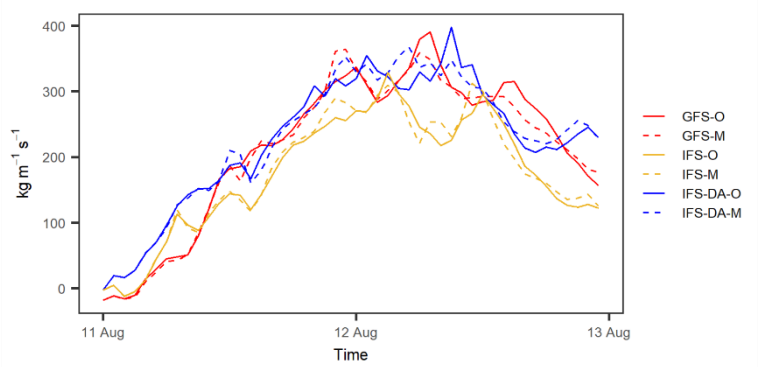

Fig. 9. Time evolution from 00 UTC 11 August 2015 to 00 UTC 13 August 2015 of the vertically integrated water vapour flux (kg m^{-1} s^{-1}) crossing section A-A' shown in Fig. 3b.

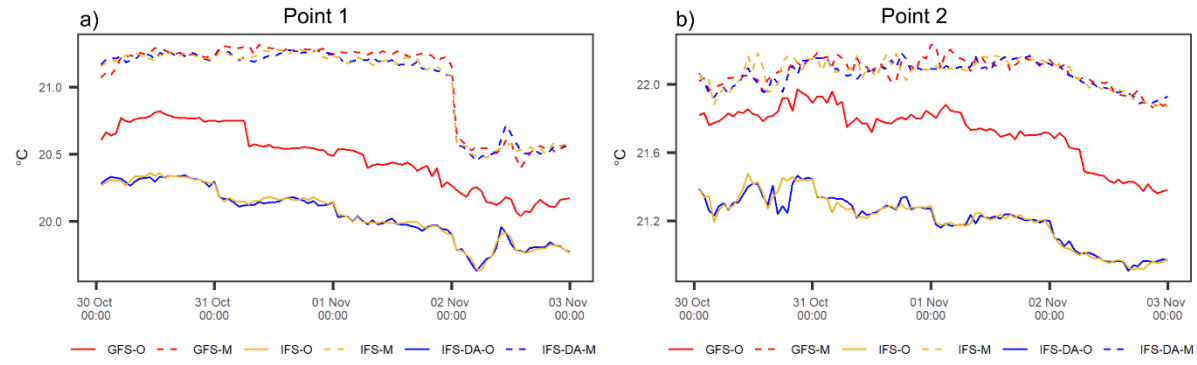

Fig. 10. Case study 2: temporal evolution of SSTSK (°C) at points 1 and 2 highlighted in Fig 3b.

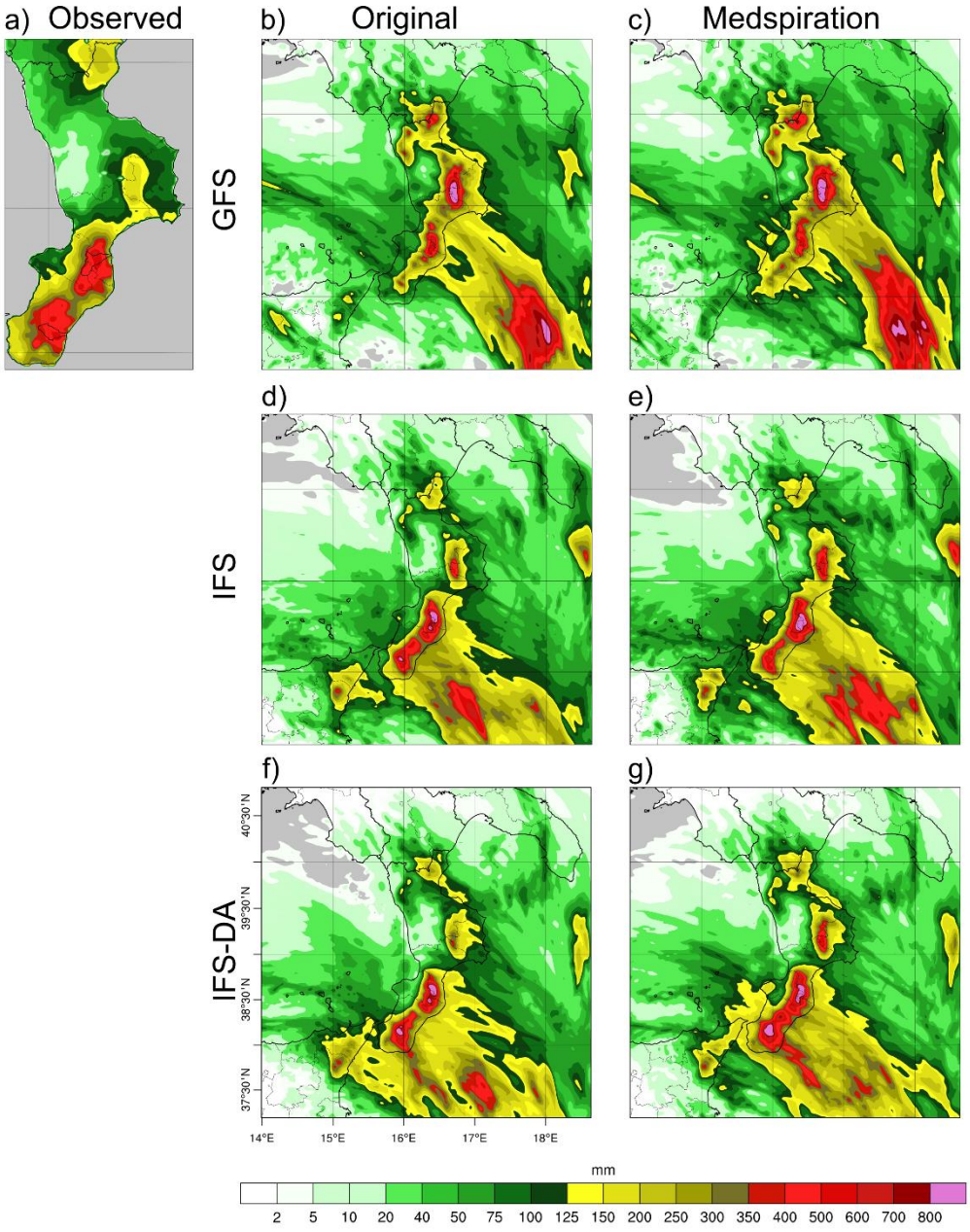

Fig. 11. Accumulated precipitation (mm) over the whole period of 96 hours starting from 00 UTC 30 October 2015: a) merged ground measurements and radar observations; b-g) simulated fields with the different configurations.

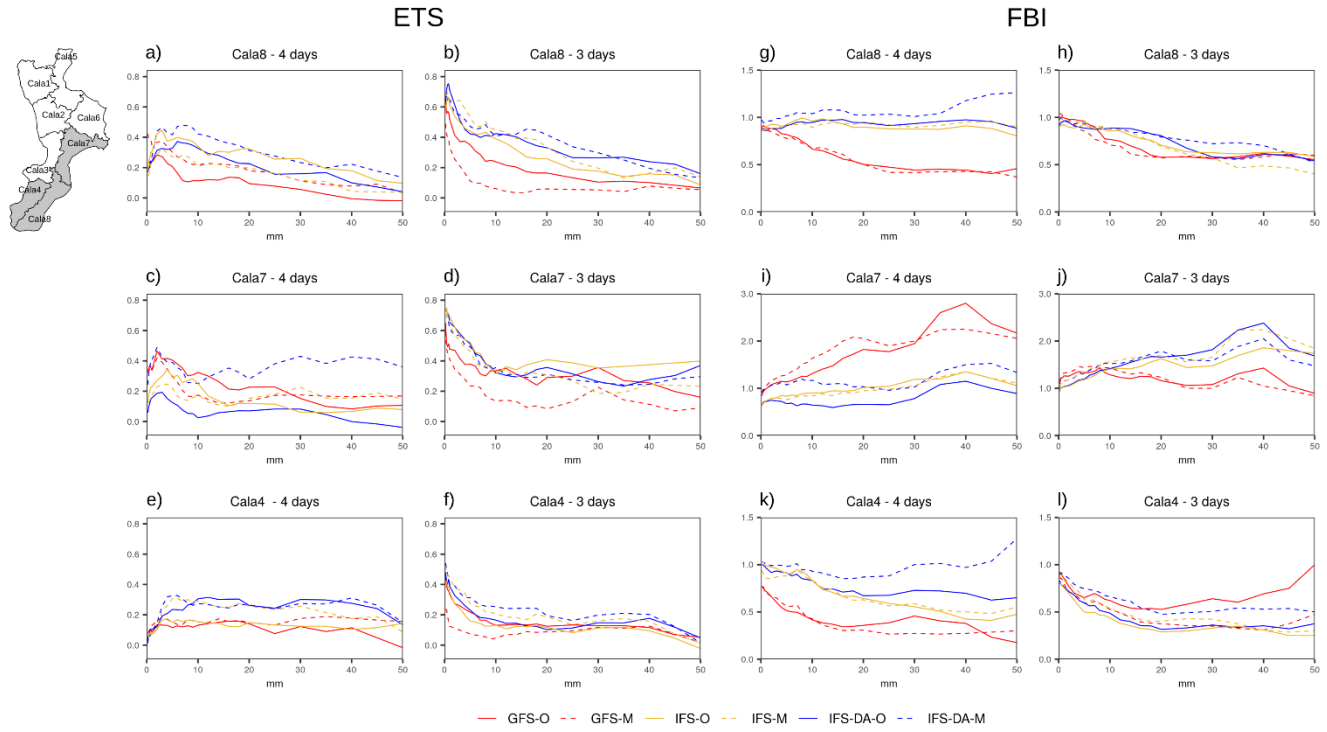

Fig. 12. Categorical scores ETS (Equitable Threat Score) (a-f) and FBI (Frequency Bias Index) (g-l) calculated on the rain gauges located in the three Civil Protection warning areas more affected by the event of case study 2 (highlighted as grey areas in the map at the top left) for both the 4-days and the 3-days period.

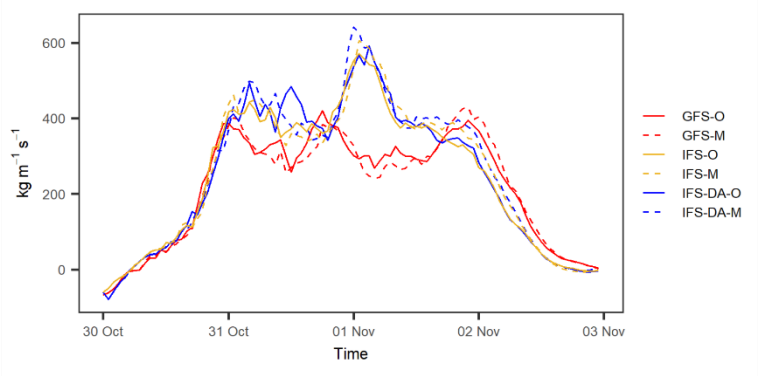

Fig. 13. Time evolution from 00 UTC 30 October 2015 to 00 UTC 3 November 2015 of the vertically integrated water vapour flux (kg m^{-1} s^{-1}) crossing section B-B' shown in Fig. 3b.

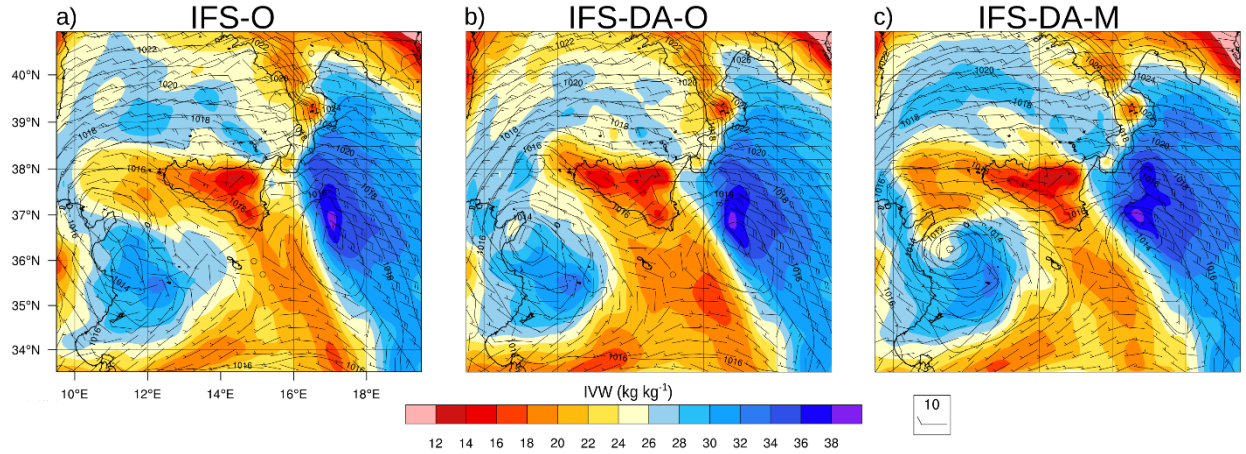

Fig. 14. Same as Fig. 8, at 21 UTC 31 October 2015.

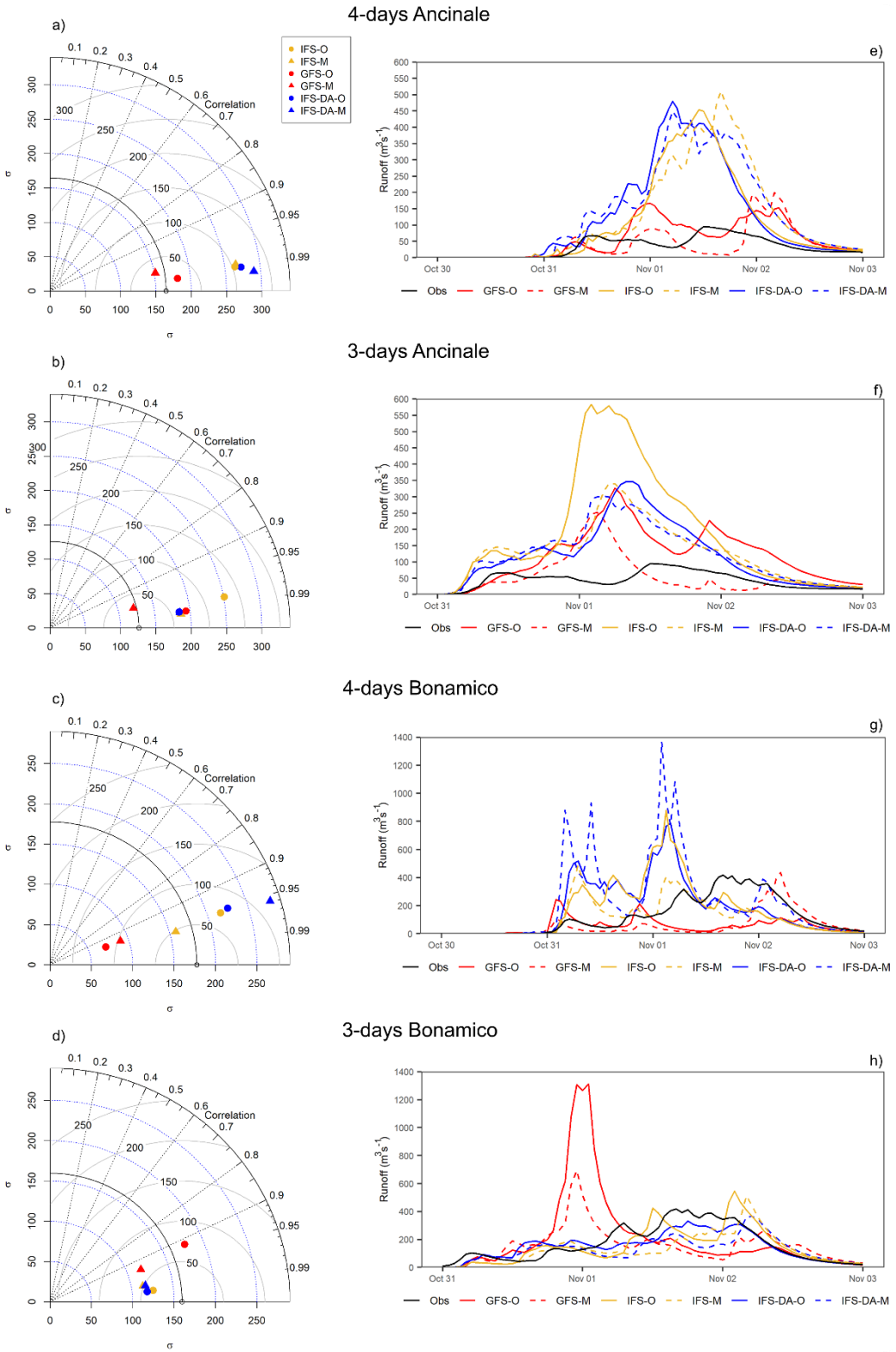
4-days Ancinale
a)
IFS-O
IFS-M
GFS-O
GFS-M
IFS-DA-O
IFS-DA-M
Correlation
σ
e)
Runoff (m3s-1)
Oct 30
Oct 31
Nov 01
Nov 02
Nov 03
Obs
GFS-O
GFS-M
IFS-O
IFS-M
IFS-DA-O
IFS-DA-M
3-days Ancinale
b)
f)
4-days Bonamico
c)
g)
3-days Bonamico
d)
h)

Fig. 15. (a-d) Taylor diagrams related to the averaged hourly precipitation series over the Ancinale River catchment and the Bonamico Creek catchment simulated by the different configurations forecasting both 4 and 3 days, compared to observations; (e-h) resulting hydrographs (m s^{-3}) obtained by the different WRF-Hydro simulations compared to observations.

TABLES

Table 1. Main WRF physical options selected for the study.

Component	Scheme Adopted
Microphysics Scheme	2 - Lin-Purdue (Chen and Sun, 2002)
PBL Scheme	2 - MJY (Mellor and Yamada,1982)
Shortwave Radiation Physics Scheme	1 - Dudhia (Dudhia, 1989)
Longwave Radiation Physics Scheme	1 - RTTM (Mlawler et al. 1997)
Land Surface Model	2 - Unified NOAH (Tewari et al., 2004)
Surface Layer	2 - Eta Similarity (Janjic, 1994)
Cumulus Physics Scheme	1 - Kain-Fritsch (only D01) (Kain, 2004)

Table 2. List of simulations with related acronyms.

ID	GCM	SST Source
GFS-O	GFS 0.25° Forecast	Original
GFS-M		Medspiration
IFS-O	IFS-ECMWF Forecast	Original
IFS-M		Medspiration
IFS-DA-O	IFS-ECMWF Forecast	Original
IFS-DA-M	3DVAR Assimilation	Medspiration

Table 3. Calibrated parameters of the off-line WRF-Hydro model for the Ancinale River and the Bonamico Creek.

Parameter	Ancinale	Bonamico
REFKDT	0.7	0.4
SLOPE	0.30	0.30
Z1 (m)	0.2	0.1
Z2 (m)	0.5	0.2
Z3 (m)	1.20	0.5
Z4 (m)	2	0.9
OVROUGHRTFAC	50	50
RETDPRTFAC (mm)	0	15
Manning's roughness coefficient 1st order	0.1	0.1
Manning's roughness coefficient 2nd order	0.062	0.063
Manning's roughness coefficient 3rd order	0.048	0.045
Manning's roughness coefficient 4rt order	0.033	0.031

Table 4. Accumulated rainfall between 02-08 UTC, simulated peak flow and peak flow time in the Citrea Creek for the different model configurations.

	GFS-O	GFS-M	IFS-O	IFS-M	IFS-DA-O	IFS-DA-M
Accumulated precipitation between 02– 08 UTC (mm)	0.0	0.7	15.8	5.3	1.1	1.4
Peak Flow (m^3s^{-1})	0.005	0.002	0.132	0.048	0.006	0.006
Peak Flow Time (UTC)	03	03	05	05	03	03

Table 5. Synoptic table summarizing the main findings for the different case studies. Acronyms: Medsp: Medspiration BC: boundary conditions. CP: Civil Protection.

	Case Study 1	Case Study 2	
	11-12 Aug (48h)	30 Oct – 2 Nov (96h)	31 Oct – 2 Nov (72h)
Skin SST fields	Generally small differences (slightly higher values with GFS and lower with Medsp), but strong IFS underestimation along coastlines.	Strong IFS underestimation along coastlines. Average Medsp values higher than GFS (about from 0.6 to 0.8 K) and IFS (> 0.8 K, even not considering IFS underestimation along coastlines). Also, with GFS underestimation along coastlines, but overestimation off the Tyrrhenian Sea.	
Precipitation amount and spatial pattern	Average rainfall increases in domain D02 moving from IFS to GFS to IFS-DA. GFS rainfall centred to the south-east, IFS and DA show more elongated shapes in the south-north direction. Medsp effect is minor with respect to varying GCM or including DA.	More rainfall in D02 with GFS. Moving from GFS to IFS to IFS-DA, a shift of the biggest rainfall cluster over the sea is observed from north-east to south-west direction. Medsp fields increase average precipitations (about 10%) but do not affect spatial patterns significantly.	GFS-based simulations are closer to the IFS-based. Medsp fields increase average precipitations (about 10%) but do not affect spatial patterns significantly.
Precipitation timing and scores	Close to the Corigliano rain gauge, GFS-based simulations delay the event. Ingesting Medsp fields accelerate flow dynamics, especially in IFS-based simulations.	Globally, better performances with IFS-DA-M in the 3 CP warning areas analysed. Relevant over- or underforecasts with GFS-based simulations. Medsp fields especially useful to improve the 3DVAR scheme, but do not change the timing of the event.	Scores of GFS-based simulations still worse, even with Medsp fields. Also, for IFS-based simulations, Medsp effect is less relevant and not always positive. Substantial over- or underforecasts with almost all simulations.
Hydrological impact	Not feasible, because no simulation can forecast reliable precipitation values for the Citrea catchment.	QPF analysis at the catchment scale: for Ancinale River, overforecast with IFS-based simulations, GFS-based much better; for Bonamico Creek, GFS-based underforecast, IFS-based better. Hydrographs, Ancinale: most IFS-based simulations are reasonably correlated with observations (but discharge overforecast), peak flow times close to observed; in GFS-based, volumes closer to observations but peak flow times are not well forecasted. Hydrographs, Bonamico: all hydrographs are not well	QPF analysis at the catchment scale: for Ancinale River, GFS-M is the best simulation, while IFS-based simulations overforecasts are reduced; for Bonamico Creek, GFS-based forecasts bias is reduced, but overall better performances with IFS-based (Taylor diagram). Hydrographs, Ancinale: results similar to 4-day forecasts, best performances with IFS-DA-O. Hydrographs, Bonamico: IFS-based simulations well correlated, peak flow times well forecasted (especially IFS-DA-O). GFS-based simulations poorly

	correlated with observations, peak flow times not well forecasted.	correlated, early forecast of the peak flow.